NACA

RESEARCH MEMORANDUM

EFFECTS OF SURFACE ROUGHNESS AND EXTREME COOLING ON BOUNDARY-LAYER TRANSITION FOR 15° CONE-CYLINDER IN FREE FLIGHT AT MACH NUMBERS TO 7.6

By Leonard Rabb and Milan J. Krasnican

Lewis Flight Propulsion Laboratory
Cleveland, Ohio

NATIONAL ADVISORY COMMITTEE
FOR AERONAUTICS

WASHINGTON

March 5, 1958
Declassified October 16, 1961

NACA RM E57K19

NATIONAL ADVISORY COMMITTEE FOR AERONAUTICS

RESEARCH MEMORANDUM

EFFECTS OF SURFACE ROUGHNESS AND EXTREME COOLING ON BOUNDARY-LAYER TRANSITION FOR 15° CONE-CYLINDER IN FREE FLIGHT AT MACH NUMBERS TO 7.6

By Leonard Rabb and Milan J. Krasnican

SUMMARY

Three cone-cylinder bodies were flown to obtain boundary-layer-transition data at very low ratios of wall to local stream temperature. Surface finishes were nominally 2-, 20-, and 50-microinch average roughness height. The smooth-body (2-microin. surface) transition data were in excellent agreement with previous smooth-body results. Laminar boundary layers were maintained to a local temperature ratio of 0.35 for this body. On the two rough models, transition occurred under conditions generally believed to be favorable for maintaining laminar flow; that is, the local Reynolds numbers were either decreasing or constant and the local temperature ratios were decreasing. This "transition reversal" phenomenon was originally described by Jack, Wisniewski, and Diaconis for smooth bodies and bodies with uniformly distributed roughness. The transition data of the two rough models qualitatively confirm their results. Turbulent heat-transfer data were in good agreement with theoretical turbulent Stanton numbers when heat-transfer reduction due to tip blunting was considered.

The maximum free-stream Mach number for these flights was 7.6, and the maximum Reynolds number (uncorrected for blunt-tip effects) at which laminar flow was observed was 46.3×10^6.

INTRODUCTION

Various problems of high-speed flight have been studied by the NACA Lewis laboratory through the use of the free-flight technique. In particular, this technique has been used to investigate the phenomenon of boundary-layer transition and related aerodynamic heating problems. Two free-flight bodies of the same design as those used in the present investigation have been flown and the results are reported in references 1 and 2. These studies show that slender models with surface finishes of the order of 2-microinch average roughness can sustain laminar flow at Reynolds

numbers as high as 50×10^6 (ref. 2) based on sharp-tip local conditions. Transition conditions agreed with wind-tunnel results (ref. 3) when the local conditions were corrected for tip bluntness.

The present tests investigated the effects of surface finish on boundary-layer transition under conditions of extreme cooling with three models of 2-, 20-, and 50-microinch average roughness height. The smooth model (2-microin. surface) duplicated the flight reported in reference 1, but the instrumentation was more extensive. The results of these flight tests are reported herein, and the data are compared with previous experimental and theoretical results.

APPARATUS AND PROCEDURE

Apparatus

The test body shown in figure 1 is typical of the three models flown in the present investigation. The design details are given in reference 1. The test bodies reported herein are designated models 3, 4, and 5; flight data for models 1 and 2 are reported in reference 1 and 2, respectively. Table I summarizes the physical characteristics of each model, and table II gives the performance data of the booster and sustainer rockets. The location of the instrumentation and the skin thickness at each instrument station are shown in figure 2. The instrumented forebodies are shown in figure 3. The three models had identical instrumentation as follows:

Measurement	Range
Skin temperature, ^{o}R	[a]400 to 1400
Flared-afterbody pressure, lb/sq in. abs	1 to 15
Nose pressure, lb/sq in. abs	1 to 275
Axial acceleration, g's	0 to 90
Axial acceleration, g's	0 to -25

[a]Model 4, 400^{o} to 1600^{o} R.

The surface finishes of the three models are listed in table III; the methods of surface finishing and measuring surface roughness are discussed in appendix A. Photographs and photomicrographs of the surface finishes are presented in figure 4.

Procedure

Each model was air-launched from an F2H-2B airplane at an altitude of approximately 45,000 feet and allowed to fall in a zero-lift trajectory. The models were accelerated to design speed by booster and sustainer rockets. All the data were transmitted to NACA ground receiver stations at Wallops Island, Virginia by means of a radio-telemetering package housed in the cone-cylinder forebody. This procedure was identical to that discussed in references 1 and 2.

The data-reduction procedure was similar to the method described in reference 4. However, the data herein are presented in terms of local flow properties, which are based on an assumed static-pressure distribution for cone-cylinder bodies of revolution given in reference 5. The local total pressure was computed from the free-stream Mach number and the normal-shock relations given in reference 6. This procedure for calculating local flow conditions was based on the method of reference 7.

RESULTS AND DISCUSSION

The primary data and the local flow conditions are discussed in appendix B.

Heat-Transfer Coefficients

The heat-transfer coefficients were determined from the time derivative of the measured skin temperatures and the heat capacity of the skin. Figures 5, 6, and 7 present these coefficients as nondimensional Stanton numbers St. Also shown are theoretical laminar and turbulent values of the Stanton numbers based on the local flow conditions and references 8 to 13.

Values of theoretical laminar Stanton numbers are not changed significantly by the assumptions of local flow conditions and are in good agreement with the laminar data of models 3, 4, and 5. However, as pointed out in references 2 and 14, tip blunting may reduce turbulent heat transfer as much as 40 percent. The good agreement of the turbulent data of models 3 and 5 with the reduced theoretical turbulent values (based on local flow properties) indicates that the predicted heat-transfer reduction was realized. However, the turbulent data of stations 10 and 11 of model 4 do not show such good agreement. Theoretical values of Stanton number were based on an arbitrary reference length for Reynolds number, which was the wetted-surface distance from the stagnation point to the temperature measuring station. The local Stanton numbers of model 4 (fig. 6) are not presented beyond 25 seconds because the model had decelerated to subsonic Mach numbers. Also, some data near

20 seconds were omitted in figure 6 because the skin temperatures were near peak values and heat transfer was near zero at this time. The Stanton numbers presented for station 1 of model 4 are not considered reliable because of a heat-sink effect of the 3-pound ballast added to the nose.

Boundary-Layer Transition

Transition data were obtained from the Stanton numbers presented in figures 5 to 7, and are summarized in table IV. The boundary layer was assumed to have a discrete point of transition, which was taken as the initial deviation of the Stanton numbers from the laminar values. In some cases (especially for model 5) the local Stanton numbers did not indicate a distinct transition point. Boundary-layer-transition points were observed during each flight for each station with the following exceptions: stations 1, 2, and 3 of model 3; station 1 of model 5; and stations 10 and 11 of models 3, 4, and 5. Stations 10 and 11 remained turbulent throughout each flight. The increases in Stanton numbers that occurred near 13 seconds for stations 1, 2, and 3 of model 3 (fig. 5(a)) were not considered to be transition points since the Stanton numbers returned to laminar values at 13.6 seconds. Also, the temperature-time histories (fig. 27(a)) indicate that the increase in Stanton numbers may have been the result of curve-fairing difficulties at 13 seconds.

Although the three test models experienced similar flight conditions, they did not show similar transition points. The highly polished surface of model 4 maintained a laminar boundary layer at local temperature ratios as low as 0.35. (Two stations on model 4 indicated early transition and will be discussed later.) However, models 3 and 5 (rough surface) indicated turbulent boundary layers at local flow conditions where laminar flow might be expected. Transition occurred while the ratios of wall to local stream temperature were decreasing and the local Reynolds numbers were either decreasing or constant. This phenomenon of transition reversal is discussed in reference 15 and is qualitatively substantiated by the transition data of models 3 and 5.

Model 4 (2-microin. average roughness). - The highly polished surface of model 4 maintained a laminar boundary layer at a ratio of wall to local stream temperature t_w/t_δ as low as 0.35. The transition-reversal phenomenon was not observed. The local temperature ratios are shown in figure 8 as a function of the local Mach number. Theoretical temperature ratios for stability at very large Reynolds numbers from reference 16 are also shown.

The minimum values of t_w/t_δ occurred near peak local Mach numbers M_δ. Typical values of minimum t_w/t_δ and the corresponding values of M_δ, Re_δ, and Re_∞ are shown in the following table:

Location	Station	Min. t_w/t_δ	Max. M_δ	Re_δ (a)	Re_∞ (b)	Boundary layer
Cone	6	0.35	2.79	5.00×10^6	46.30×10^6	Laminar
Cylinder	7	.44	3.61	2.99	26.18	Laminar
Cylinder	9	.49	3.56	4.56	41.00	Laminar

[a]Local Reynolds number corrected for tip bluntness.

[b]Local Reynolds number based on sharp-tip conditions.

The maximum uncorrected local Reynolds number at which laminar flow was observed was as high as 46.3×10^6.

The boundary layer along the cone remained laminar until t_w/t_δ and M_δ (fig. 8) approached the theoretical limits of reference 16. However, stations 8 and 9 became turbulent for a short time at local conditions that were theoretically stable to very large Reynolds numbers (fig. 8(b)). It is unlikely that this might be transition reversal, as discussed in reference 15, because the turbulent boundary layer became laminar as local cooling became more severe. The possibility that momentary angle of attack affected stations 8 and 9 is also unlikely, because the turbulent flow occurred during the most stable part of the flight trajectory. There is no reasonable explanation at present for the early-transition data of stations 8 and 9.

Figure 9 presents the variation of t_w/t_δ with local Reynolds numbers. Smooth-body transition data from references 1, 3, and 17 are also shown. Transition at all stations except the early transitions at stations 8 and 9 (fig. 9(b)) was in excellent agreement with the reference data.

A summary of the smooth-body transition data of model 4 and references 1, 3, and 17 is presented in figure 10. Converting the local stream conditions from sharp tip to blunt tip reduced the peak transition Reynolds number from 32.9×10^6 to 11.5×10^6. Maximum uncorrected Reynolds numbers of 46.3×10^6 were observed on the cone with a laminar boundary layer earlier in the flight.

Models 3 and 5 (50- and 20-microin. average roughness). - The flights of models 3 and 5 were not as long as that of model 4 because of component malfunctions, but both models experienced transition. The local

temperature ratios for models 3 and 5 are plotted against local Mach number and Reynolds number in figures 11 to 14. Minimum local temperature ratios for models 3 and 5 occurred at peak local Mach numbers. Typical values of minimum t_w/t_δ and the corresponding values of M_δ, Re_δ, and Re_∞ are given in the following table:

Location	Station	Min. t_w/t_δ	Max. M_δ	Re_δ (a)	Re_∞ (b)	Boundary Layer
Model 3 (50-microin. average roughness)						
Cone	4	0.38	2.81	3.48×10^6	34.12×10^6	Turbulent
Cylinder	7	.54	3.50	3.40	25.72	Turbulent
Cylinder	9	.54	3.59	4.75	43.98	Turbulent
Model 5 (20-microin. average roughness)						
Cone	4	0.66	2.47	3.31×10^6	13.18×10^6	Turbulent
Cylinder	7	.86	2.84	4.02	12.92	Turbulent
Cylinder	9	.81	2.98	5.54	23.58	Turbulent

[a]Local Reynolds number corrected for tip bluntness.

[b]Local Reynolds number based on sharp-tip conditions.

Figures 13 and 14 show that transition occurred under conditions that might be expected to maintain a laminar boundary layer. The local temperature ratios were decreasing and the Reynolds numbers were either decreasing or nearly constant. The values of t_w/t_δ at transition for models 3 and 5 were below the theoretically stable values of reference 16 (see figs. 11 and 12) and below the experimental stability-limit curve for smooth bodies from references 1, 3, and 17 (figs. 13 and 14). Also shown in figures 13 and 14 are some transition curves in the reversal region from reference 15 for similar values of local Reynolds number per foot and surface finish. Although the data of model 3 are in excellent agreement with the data of reference 15, uncertainties as to the true surface finish of model 3 (see appendix A) make quantitative comparisons doubtful. The data do confirm, however, the sensitivity of transition to local temperature ratio rather than local Reynolds number. The same trend is confirmed for model 5 (fig. 14). However, the transition curve of the present data did not agree with the data of reference 15 (fig. 14), and further data are needed to explain the transition phenomenon in the reversal region.

Figure 15 shows that transition reversal occurred at higher local temperature ratios for model 5 than for model 3. This was very surprising because the nominal surface finish of model 5 was 20 microinches as

compared with 50 microinches for model 3. Wind-tunnel tests (ref. 15) have indicated that the effect of increased surface roughness is to raise the temperature ratio at which reversal occurs.

The apparent inconsistency in the results of models 3 and 5 suggested that the type of surface finish may be as important as the average value of surface roughness. (See appendix A.) The photographs in figure 4 show that the finishes of the two rough bodies were indeed different. Furthermore, the photographs in figure 3 and the "feel" of each surface indicated that model 3 had a "smoother" surface than model 5. From this viewpoint, the transition data of models 3 and 5 were consistent with the trend discussed in reference 15.

The temperature ratios for the transition points shown in figure 15 are higher for the cylinder stations than for those along the cone. For example, t_w/t_δ for model 3 was approximately 0.65 along the cylinder and 0.45 along the cone. This trend may have been a local Mach number effect, as M_δ was greater along the cylinder than along the cone. Tabulated values of local Reynolds number per foot Re_δ/ft are also given in figure 15. Decreasing Re_δ/ft from cone values to cylinder values would tend to reduce t_w/t_δ at transition (see ref. 15). Consequently, if t_w/t_δ at transition were sensitive to local Mach number, the effect would be partly masked by the change in local Re_δ/ft around the cone-cylinder. It should be recognized that other factors, such as pressure gradient, may also influence transition around the cone-cylinder.

SUMMARY OF RESULTS

The smooth-body data of this report together with earlier flight data for smooth bodies have shown that slender bodies can sustain laminar boundary layers at very high Reynolds number (50×10^6), and extremely low local temperature ratios (0.25). However, for the rough models of this investigation, transition was encountered during acceleration at nearly constant or decreasing Reynolds number with decreasing local temperature ratio. The adverse effect of extreme cooling in the presence of roughness has therefore been demonstrated in flight and is in qualitative agreement with the wind-tunnel results of Jack, Wisniewski, and Diaconis.

Smooth-Body Results

1. The highly polished surface (2-microin. average roughness) maintained a laminar boundary layer under conditions of extreme boundary-layer cooling. Ratios of wall to local stream temperature as low as

0.35 were observed without transition reversal occurring. The local Reynolds number corrected for blunting effects was 5.0×10^6 and uncorrected was 46.3×10^6.

2. Boundary-layer transition was observed along the cone and cylinder at local flow conditions that were in excellent agreement with previous smooth-body results in wind tunnels and flight.

3. Transition occurred at two stations very early in the flight and at local flow conditions that were well within the theoretical stability limits. No satisfactory explanation of this phenomenon is known.

Rough-Body Results

1. Two bodies of nominal surface roughness of 20- and 50-microinch average roughness were flown at local conditions well within theoretical stability limits. Transition was observed at these conditions while the local wall-to-stream temperature ratio was decreasing and the local Reynolds number per foot was either constant or decreasing. The boundary layer remained turbulent at local temperature ratios as low as 0.38.

2. Boundary-layer transition at low local temperature ratios was considered to be evidence of the transition reversal phenomenon discussed in reference 15. The data indicated that average-surface-roughness measurements were not sufficient to describe a surface for predictions of transition in the reversal region.

3. Local Mach number may influence the temperature ratio at transition in the reversal region. Local temperature ratios at transition increased from approximately 0.45 on the cone to 0.65 on the cylinder for the 20-microinch surface finish. The corresponding change in local Mach number was from 2.6 to 3.0. The effect of local Mach number may have been partly masked by the decrease in local Reynolds number per foot on the cylinder.

4. The turbulent heat-transfer data agreed well with the reduced theoretical turbulent values based on local flow properties.

Lewis Flight Propulsion Laboratory
National Advisory Committee for Aeronautics
Cleveland, Ohio, December 5, 1957

APPENDIX A

DISCUSSION OF MODEL SURFACE FINISH

The surface roughness was measured with the Brush Surfindicator, model BL-110, which measured the arithmetic average deviation from a mean surface in microinches, called "average roughness" in this report. Surfaces having finishes of less than 10 microinches were checked with an interferometer microscope, and surfaces of less than 50 microinches were checked with a micrometrical surface tester. It is estimated that uncertainties in measurement may be as high as ±20 percent, although cross-checks between the several types of instruments usually agreed within ±10 percent. Observations indicated that any given surface had small variations in average roughness. The vapor-blast technique appeared to be superior to hand polishing in terms of a uniform finish.

Figures 4(a) to (e) show the macroscopic differences in surface texture with varying roughness. Differences in contrast are due to variations in surface illumination during photography. A qualitative "feel" or touch of the 20- and 50-microinch surfaces indicated that the 50-microinch surface of model 3 felt relatively smoother than the 20-microinch surface of model 5. Differences in polishing technique suggested further investigation. Therefore, photomicrographs (figs. 4(f) to (j)) were made. In these, there appear to be significant differences in the physical nature of the surfaces, dependent on the manner in which the roughness was obtained. For example, in model 3 (figs. 4(f) and (g)) the dark areas represent holes in the surface made with the initial vapor-blast treatment (100-microin. average roughness). Successive hand polishing with sandpaper smoothed the rough surface to an average roughness of 50 microinches. One can see the flat areas (reflecting light) and note that they are considerably smoother than the corresponding areas that were vapor-blasted to an average roughness of 20 microinches on model 5 (figs. 4(i) and (j)). Profile photomicrographs (figs. 4(k) and (l)) of model 3 (50-microin.) indicate that the surfaces between craters or depressions are relatively smoother and longer than those on model 5, which was vapor-blasted to an average roughness of 20 microinches (figs. 4(n) and (o)). Consequently, average roughness height alone is not adequate to describe surface finish, since different types of roughness may yield the same average value. The kind of surface roughness, the polishing technique, and the average roughness height should all be considered important factors.

The foregoing explanation may account for the earlier transition observed on model 5 (20-microin. surface), which was relatively smooth compared with the rougher body of model 3 (50-microin. surface). A systematic investigation of the effect of type of surface as well as the effect of average surface roughness on transition will be required to confirm this explanation.

APPENDIX B

PRIMARY DATA AND LOCAL CONDITIONS

Primary Data

The primary data for the three models are presented as time histories in figures 16 to 32. The flight conditions of models 3, 4, and 5 were very similar during the accelerating part of the flight.

The accelerations shown in figure 17 were approximately 20 g's during the initial rocket boost stage. Acceleration during the second stage of models 3 and 4 ranged from 55 to 70 g's. The increase in acceleration with time was due to the reduction in weight as the propellant burned. A maximum acceleration of 90 g's was recorded for model 5 at 11.6 seconds, which is believed to have been due to a faulty rocket motor that exploded. The flight record stopped shortly after the peak acceleration was reached. Data for model 3 were recorded up to the end of the boosting period. Large fluctuations in the acceleration data just prior to the end of the flight (not shown in fig. 17) indicated that the model had tumbled, probably because of aerodynamic instability. A 3-pound ballast was added to model 4, and the increased flight time is attributed to the increased stability at peak Mach number. Data were recorded during the boost phase and during the complete coasting flight for model 4.

The maximum free-stream Mach numbers (fig. 19) were 7.6, 7.2, and 5.1 for models 3, 4, and 5, respectively. The corresponding maximum free-stream Reynolds number per foot for each model was 20.8×10^6, 18.8×10^6 and 10.4×10^6 (fig. 20). Free-stream total temperatures are shown in figure 21. A peak temperature of 4380° R was calculated for model 3.

Local Stream Conditions

Local stream Reynolds number per foot Re_δ/ft and local Mach number M_δ are presented in figures 22, 23, and 24 for models 3, 4, and 5, respectively. The values of Re_δ/ft and M_δ are considerably less than the free-stream values because of the hemispherically blunted tip. All local stream conditions have been corrected for tip bluntness by the method of reference 7. Local stream conditions were based on an assumed static-pressure distribution over the cone-cylinder according to reference 5. However, measured pressures were used for the flared afterbody (station 11). These pressures are shown in figure 25 as the variation of local pressure ratio p_∞/p_0 with free-stream Mach number.

The local stream conditions for the three models are compared in figure 26, where M_δ is plotted against Re_δ/ft. The curves are similar for all models to the peak values of M_δ. A maximum M_δ of 3.72 is shown for model 3 at station 7. A calculated peak Re_δ/ft of 6.6×10^6 occurred at cone stations of model 4, after the model had decelerated to a free-stream Mach number of 2.1 at an altitude of 21,000 feet.

Local Wall Conditions

Time histories of the measured wall temperatures are presented in figures 27, 28, and 29. Peak temperatures for models 3 and 5 were considerably lower than those of model 4 because of the short flight times involved. The measured temperatures at station 1 of model 4 were consistently lower than those at other stations along the cone (fig. 28(a)). The additional ballast was located near station 1 and is assumed to have acted as a heat sink. Consequently, the data for this station are not considered reliable.

The ratios of wall to local stream temperature t_w/t_δ are plotted against time in figures 30, 31, and 32. Values of t_w/t_δ range from a minimum of 0.30 at station 3 of model 3 (fig. 30(a)) to a maximum of 2.16 at station 2 of model 4 (fig. 31(a)). The local stream temperature t_δ at each station was also corrected for tip-bluntness effects by the method of reference 7.

REFERENCES

1. Disher, John H., and Rabb, Leonard: Observation of Laminar Flow on a Blunted 15° Cone-Cylinder in Free Flight at High Reynolds Numbers and Free-Stream Mach Numbers to 8.17. NACA RM E56G23, 1956.

2. Rabb, Leonard, and Krasnican, Milan J.: Observation of Laminar Flow on an Air-Launched 15° Cone-Cylinder at Local Reynolds Numbers to 50×10^6 at Peak Mach Number of 6.75. NACA RM E56L03, 1957.

3. Jack, John R., and Diaconis, N. S.: Variation of Boundary-Layer Transition with Heat Transfer on Two Bodies of Revolution at a Mach Number of 3.12. NACA TN 3562, 1955.

4. Rabb, Leonard, and Simpkinson, Scott H.: Free-Flight Heat-Transfer Measurements on Two 20°-Cone-Cylinders at Mach Numbers from 1.3 to 4.9. NACA RM E55F27, 1955.

5. Clippinger, R. F., Giese, J. H., and Carter W. C.: Tables of Supersonic Flows About Cone Cylinders. Pt I: Surface Data. Rep. No. 729, Ballistic Res. Labs., Aberdeen Proving Ground (Md.), July 1950. (Proj. TB3-0108H of Res. and Dev. Div., Ord. Dept.)

6. Ames Research Staff: Equations, Tables, and Charts for Compressible Flow. NACA Rep. 1135, 1953. (Supersedes NACA TN 1428.)

7. Moeckel, W. E.: Some Effects of Bluntness on Boundary-Layer Transition and Heat Transfer at Supersonic Speeds. NACA Rep. 1312, 1957. (Supersedes NACA TN 3653.)

8. Van Driest, E. R.: Investigation of Laminar Boundary Layer in Compressible Fluids Using the Crocco Method. NACA TN 2597, 1952.

9. Van Driest, E. R.: The Turbulent Boundary Layer on a Cone in a Supersonic Flow at Zero Angle of Attack. Jour. Aero. Sci., vol. 19, no. 1, Jan. 1952, pp. 55-57; 72.

10. Cohen, Clarence B., and Reshotko, Eli: The Compressible Laminar Boundary Layer with Heat Transfer and Arbitrary Pressure Gradient. NACA Rep. 1294, 1956. (Supersedes NACA TN 3326.)

11. Reshotko, Eli: Simplified Method for Estimating Compressible Laminar Heat Transfer with Pressure Gradient. NACA TN 3888, 1956.

12. Van Driest, E. R.: Turbulent Boundary Layer in Compressible Fluids. Jour. Aero. Sci., vol. 18, no. 3, Mar. 1951, pp. 145-161.

13. Rubesin, Morris W.: A Modified Reynolds Analogy for the Compressible Turbulent Boundary Layer on a Flat Plate. NACA TN 2917, 1953.

14. Ferri, Antonio, Zakkay, Victor, and Libby, Paul A.: A Theoretical and Experimental Analysis of a New Method of Reducing Aerodynamic Heating. PIBAL Rep. 325, TN 57-113, Polytech. Inst. Brooklyn, Mar. 1957. (Contract AF-18(600)-694.)

15. Jack, John R., Wisniewski, Richard J., and Diaconis, N. S.: Effects of Extreme Surface Cooling on Boundary-Layer Transition. NACA TN 4094, 1957.

16. Dunn, D. W., and Lin, C. C.: On the Stability of the Laminary Boundary Layer in a Compressible Fluid. Jour. Aero. Sci., vol. 22, no. 7, July 1955, pp. 455-477.

17. Rabb, Leonard, and Disher, John H.: Boundary-Layer Transition at High Reynolds Numbers as Obtained in Flight of a 20° Cone-Cylinder with Wall to Local Stream Temperature Ratios near 1.0. NACA RM E55I15, 1955.

18. Moorman, Emily P.: Free-Flight Rocket Material Characteristics. Rep. No. A-10a, Tech. and Eng. Div., Ord. Missile Labs., Redstone Arsenal, Huntsville (Ala.). (Revised June 1, 1956.)

TABLE I. - PHYSICAL DATA OF TWO-STAGE TEST BODIES

Model	3	4	5
Surface finish of instrumented cone-cylinder, microin. average roughness			
Cone	50	2	20
Cylinder	50	2	20
Skin material of second stage			
Cone	Nickel	Inconel	Nickel
Cylinder	Inconel	Inconel	Inconel
Gross weight at launching (both stages less igniters), lb	235.5	239.2	239.2
Gross weight of second stage (less igniters), lb	77.0	80.0	80.0
Gross weight of booster (with coupling assembly), lb	158.5	159.2	159.2
Coupling assembly weight, lb	3.0	3.0	3.0
Weight of second stage at burnout, lb	43.28	45.7	46.1
Telemeter package weight, lb	16.0	16.2	16.2
Center of gravity at launching[1], in.	75.85	75.46	75.46
Center of gravity at first-stage burnout[1], in.	65.1	64.7	64.7
Center of gravity of second stage after separation[1], in.	41.74	40.70	40.43
Center of gravity of second stage after burnout[1], in.	38.4	36.8	36.3
Booster fin area (2 fins), sq in.	152.0	152.0	152.0
Second-stage fin area (2 fins), sq in.	24.2	24.2	24.2
Included wedge angle of second-stage wedge fin, deg	10	10	10
Body diameter of booster, in.	9.32	9.32	9.32
Body diameter of second stage, in.	6.00	6.00	6.00
Included cone angle of second stage, deg	15	15	15

[1]From nose tip.

TABLE II. - ROCKETS

[Ref. 18]

Rocket	Gross weight, lb	Propellant weight, lb	Average thrust, lb	Impulse, lb-sec	Gross-weight specific impulse, lb-sec	Propellant specific impulse, lb-sec	Burning time, sec
Sustainer (T-55)	45.8	33.5	[a]3900	[a]6,950	[a]152	[a]208	[a]1.60
Booster (T-40)	132.0	103.0	[b]3500	[b]21,000	[b]159	[b]204	[b]5.22

[a]At -20° F and sea level.
[b]At 130° F and sea level.

TABLE III. - MODEL SURFACE FINISH

Model	Forebody material		Method of cone fabrication	Method of finishing forebody surface	Average surface roughness, microin. (a)	Roughness measurement method	Afterbody	
	Cone	Cylinder					Surface material	Surface finish
3	Nickel	Inconel	Spun on lathe	Vapor-blasted to ≈100 microinch-average roughness; hand polished with wet/dry 400 grade sandpaper; final hand-polish with wet/dry 600 grade sandpaper	50	Brush Surfindicator, model BL-110	Inconel	Stock finish; chemically blackened
4	Inconel	Inconel	Spun on lathe	Polished with successively finer grades of commercial diamond paste	2	Brush Surfindicator, model BL-110 and interferometer microscope	Inconel	Stock finish; chemically blackened
5	Nickel	Inconel	Ground on lathe	Polished to 2 microinch - average roughness by commercial diamond paste; vapor-blasted to 6 microinches with 1250-mesh sand; vapor-blasted to final finish with 140-mesh sand at reduced pressure	20	Brush Surfindicator, model BL-110 and micrometrical surface tester	Inconel	Stock finish; chemically blackened

[a]Arithmetic average deviation from mean surface.

TABLE IV. - TRANSITION SUMMARY[a]

Station	Model	Time of transition, sec	t_w/t_δ	M_δ	Re_δ	Re_δ/ft	Re_θ	Comments
Cone								
1	3	----	----	----	---------	--------	----	(b)
	4	----	----	----	---------	--------	----	Heat sink at tip makes data uncertain
	5	----	----	----	---------	--------	----	(b)
2	3	----	----	----	---------	--------	----	(b)
	4	20.2	1.90	1.92	3.67×10^6	6.44×10^6	736	
	5	10.4	.70	2.24	1.74	3.04	506	
3	3	----	----	----	---------	--------	----	(b)
	4	19.5	1.65	2.05	5.23×10^6	6.10×10^6	878	Near peak temperature
	5	9.4	.83	2.02	2.59	3.05	617	
4	3	12.8	0.45	2.59	3.58×10^6	3.15×10^6	725	
	4	19.5	1.56	2.05	7.00	6.10	1012	Near peak temperature
	5	8.8	.92	1.89	3.46	3.05	713	
5	3	12.8	0.44	2.59	4.41×10^6	3.15×10^6	805	
	4	19.3	1.40	2.11	8.39	6.01	1112	
	5	8.8	.92	1.89	4.26	3.05	792	
6	3	12.8	0.45	2.59	5.19×10^6	3.15×10^6	874	
	4	19.1	1.29	2.13	9.84	5.98	1202	
	5	8.8	.92	1.89	4.95	3.05	855	
6a	3	12.4	0.54	2.49	5.50×10^6	3.34×10^6	----	
	4	19.1	1.54	2.13	9.87	5.98	----	
	5	8.6	.93	1.84	4.96	3.01	----	
Cylinder								
7	3	12.6	0.61	3.11	4.07×10^6	2.21×10^6	960	
	4	19.0	1.23	2.51	8.68	4.72	1310	
	5	8.8	1.00	2.30	4.38	2.65	944	
8	3	12.5	0.65	3.00	5.29×10^6	2.37×10^6	1164	
	4	10.4	.91	2.34	6.02	2.70	1175	
		11.3	.87	2.60	5.50	2.48	1156	
		18.6	1.10	2.52	10.03	4.50	1557	
	5	8.7	1.03	2.10	6.11	2.74	1166	
9	3	12.0	0.64	2.89	6.58×10^6	2.46×10^6	1344	
	4	10.0	.96	3.20	7.66	2.86	1386	
		11.3	.87	2.58	6.79	2.54	1344	
		18.1	1.10	2.66	11.48	4.29	1751	
	5	8.6	1.03	2.05	7.36	2.79	1361	May be turbulent at all times

[a]Based on variation of Stanton number with time.

[b]Boundary layer laminar at all times.

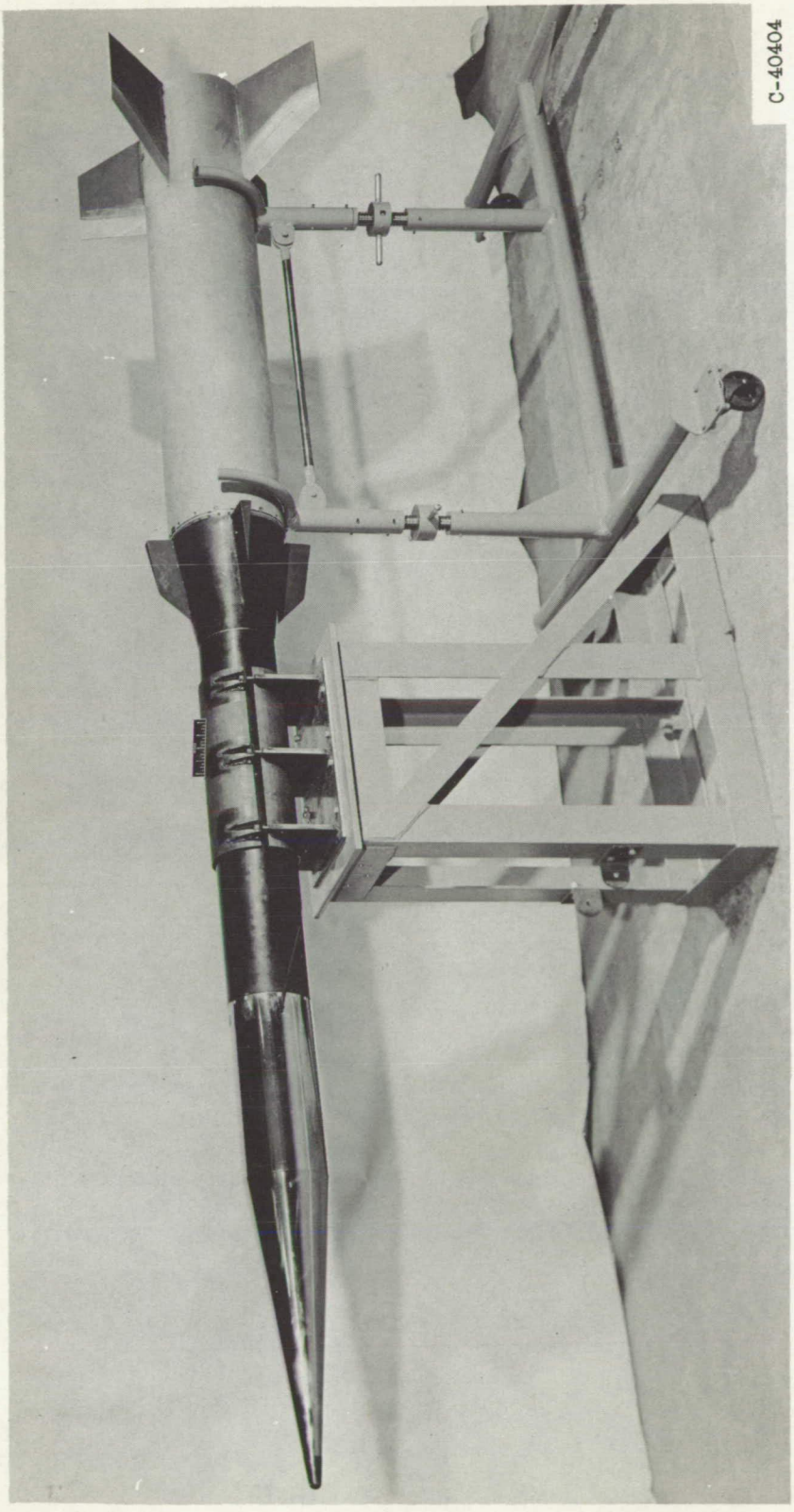

Figure 1. - Test body and booster rocket.

Station	Axial distance, in.	Wetted-surface distance, in.	α	Skin thickness, in.		
				Model 3	Model 4	Model 5
1	3.10	3.38	180°	0.055	0.027	0.055
2	6.54	6.84	184°20'	.056	.030	.053
3	9.84	10.18	180°	.056	.030	.055
4	13.25	13.60	181°14'	.057	.029	.056
5	16.40	16.77	181°21'	.057	.028	.057
6	19.32	19.73	177°39'	.057	.026	.054
6a	19.40	19.79	0°	.056	.028	.054
7	21.65	22.07	179°7'	.027	.028	.027
8	26.30	26.72	182°17'	.028	.029	.028
9	31.72	32.13	176°13'	.030	.029	.031
10	60.81	61.23	165°42'	.029	.033	.033
11	67.56	67.98	225°	.029	.033	.032

Model	Pressure tap on flared afterbody
3	Same distance as station 11, but at 45°
4	Same distance as station 11, but at 45°
5	Same distance as station 11, but at 245°

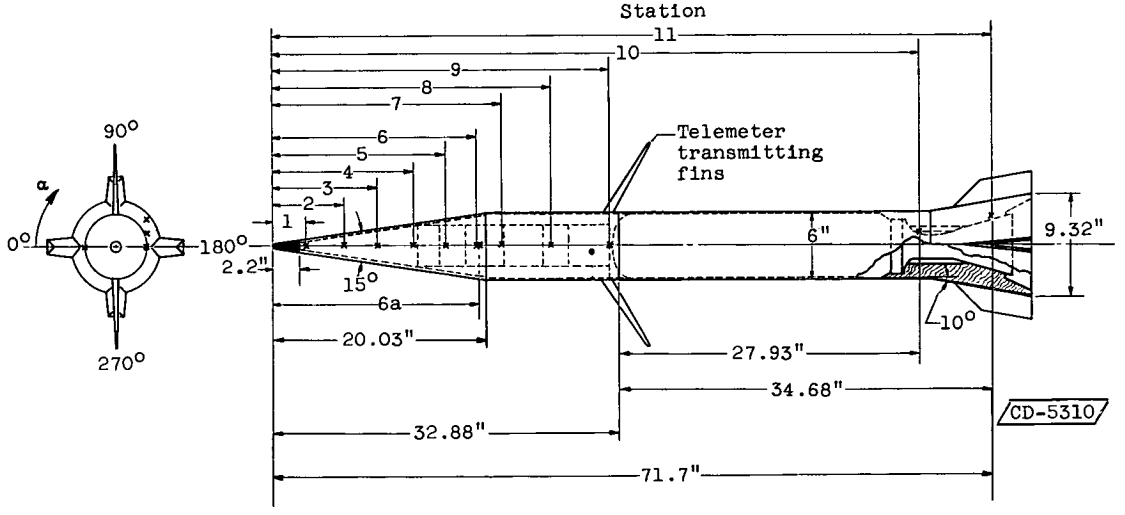

Figure 2. - Instrumentation locations and skin thickness at each station for three test models.

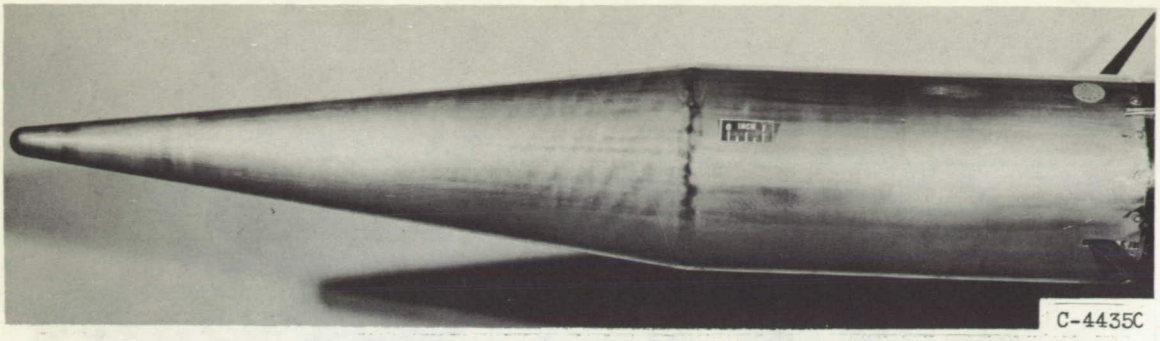

(a) Model 3, 50-microinch average roughness.

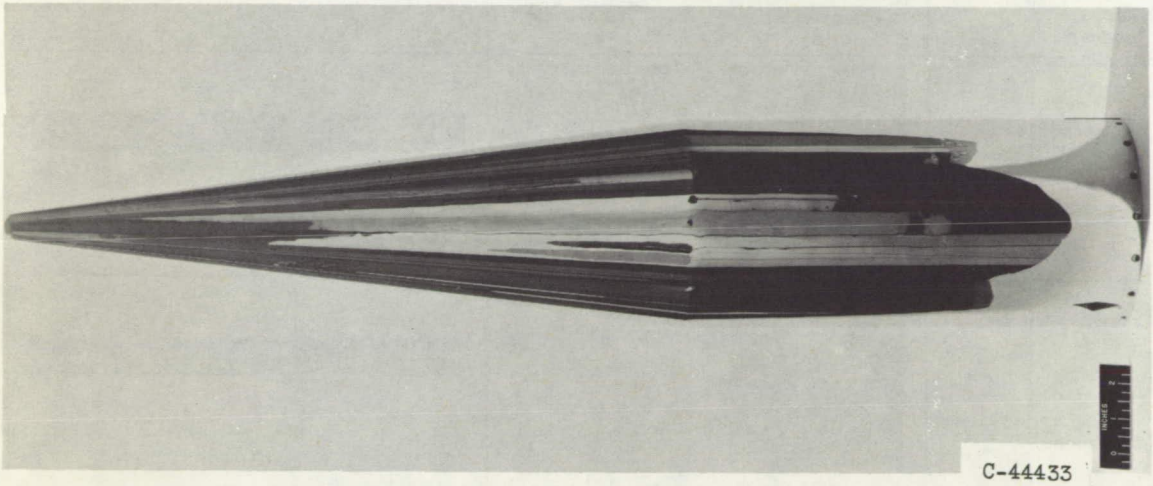

(b) Model 4, 2-microinch average roughness.

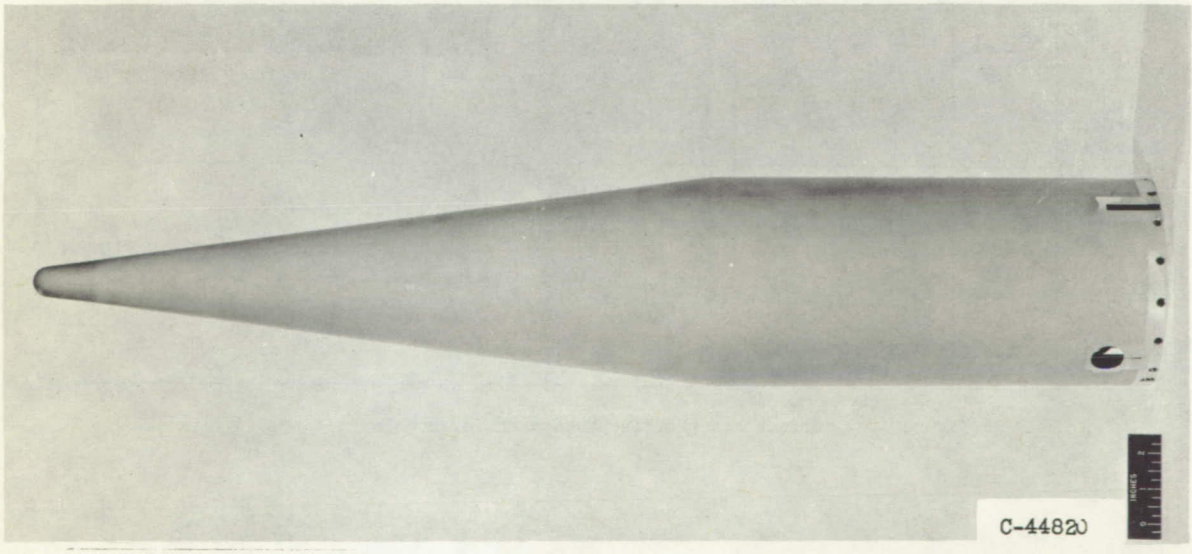

(c) Model 5, 20-microinch average roughness.

Figure 3. - Photographs of instrumented forebodies.

Model	Forebody	Surface photograph (X5)	Surface photomicrograph (X150)	Profile photomicrograph (X150)
3 (50-microin. average roughness)	Nickel cone	 (a)	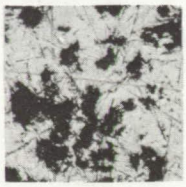 (f)	 (k)
	Inconel cylinder	 (b)	 (g)	 (l)
4 (2-microin. average roughness)	Inconel cone and cylinder	 (c)	 (h)	 (m)
5 (20-microin. average roughness)	Nickel cone	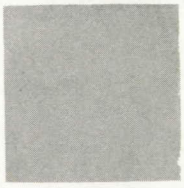 (d)	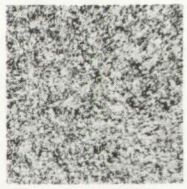 (i)	 (n)
	Inconel cylinder	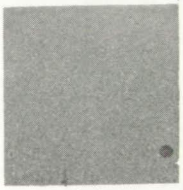 (e)	 (j)	 (o)

Figure 4. - Surface and profile photographs of models 3, 4, and 5.

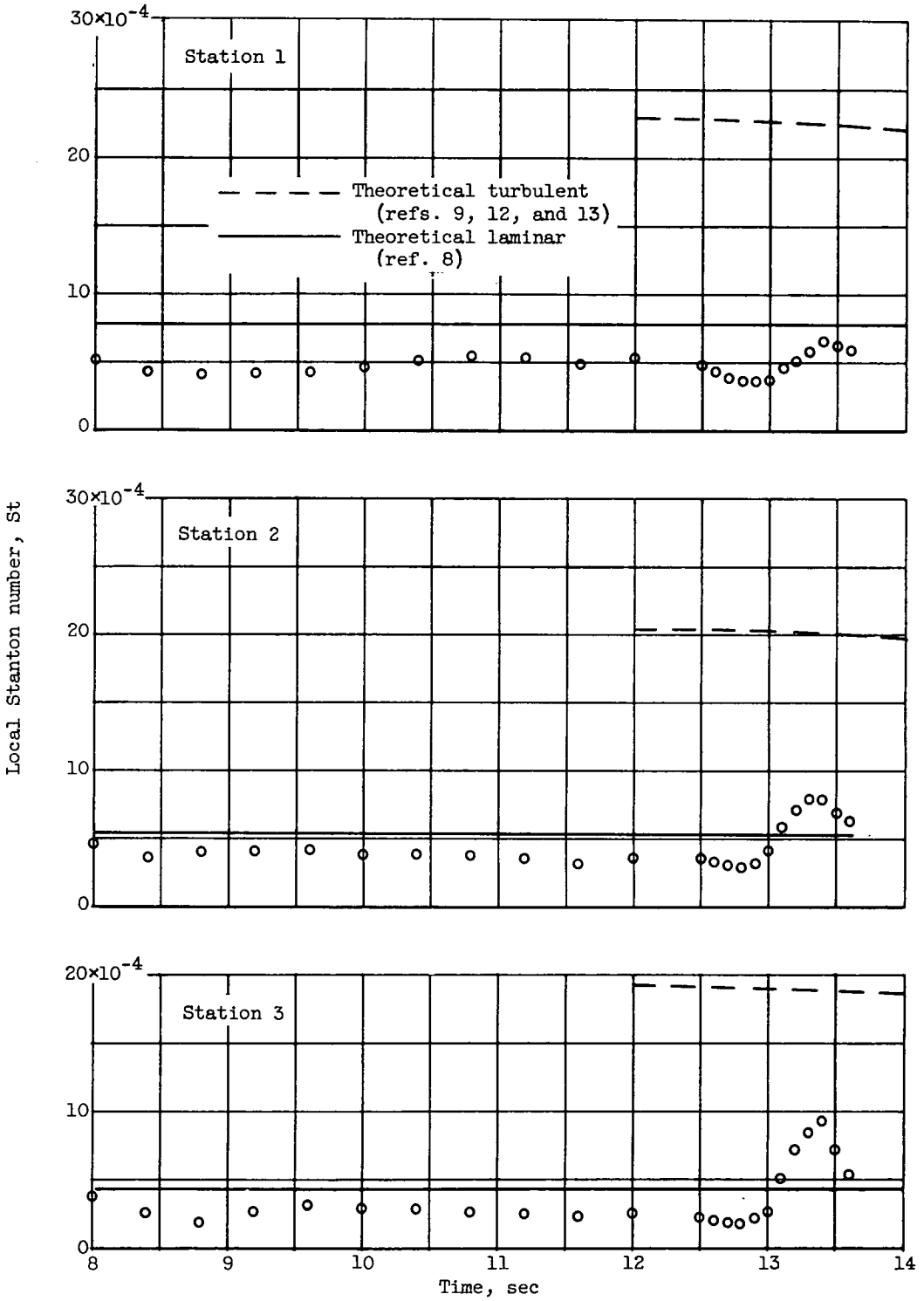

(a) Stations on cone.

Figure 5. - Time history of local Stanton number for model 3 (50-microin. average roughness).

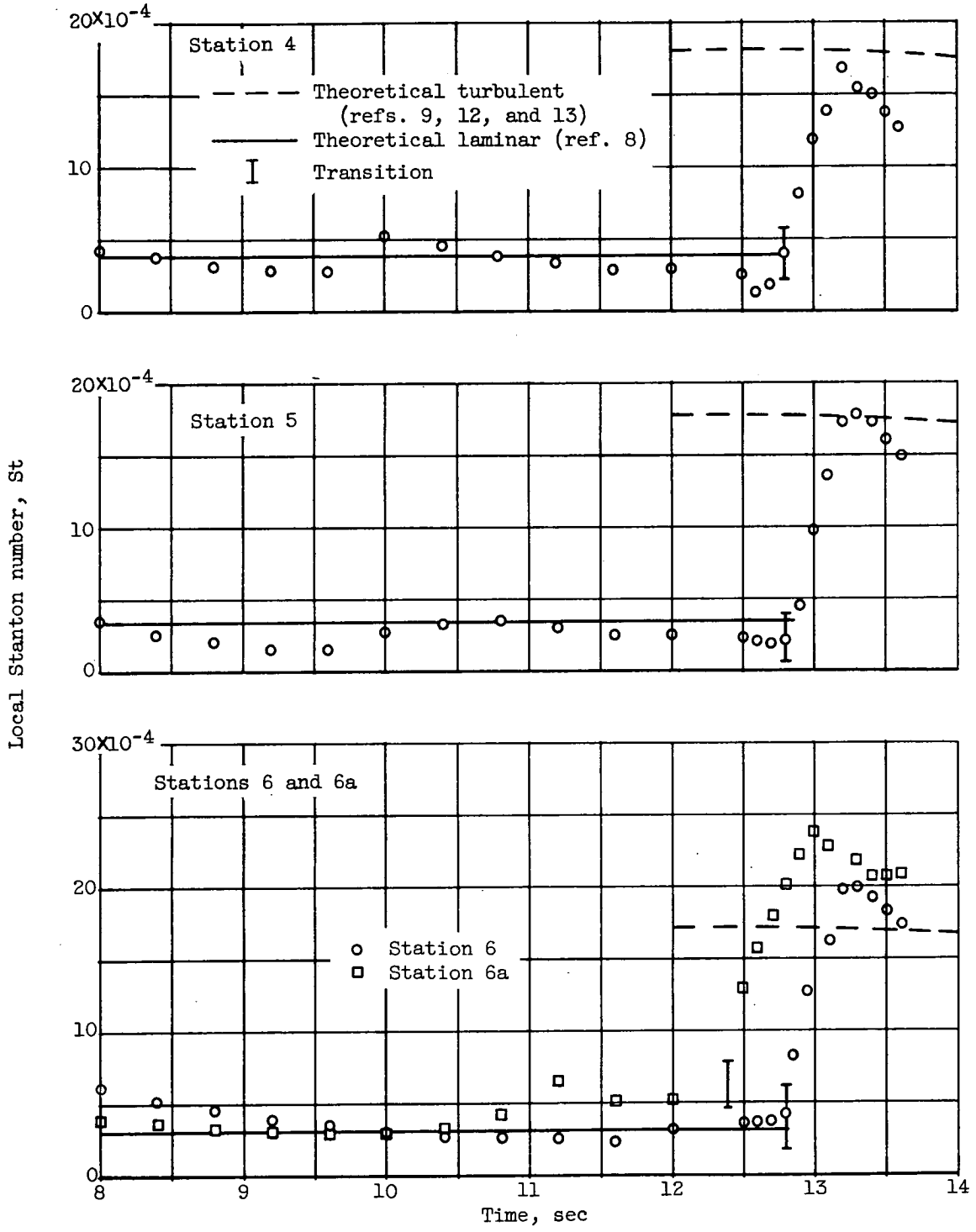

(a) Concluded. Stations on cone.

Figure 5. - Continued. Time history of local Stanton number for model 3 (50-microin. average roughness).

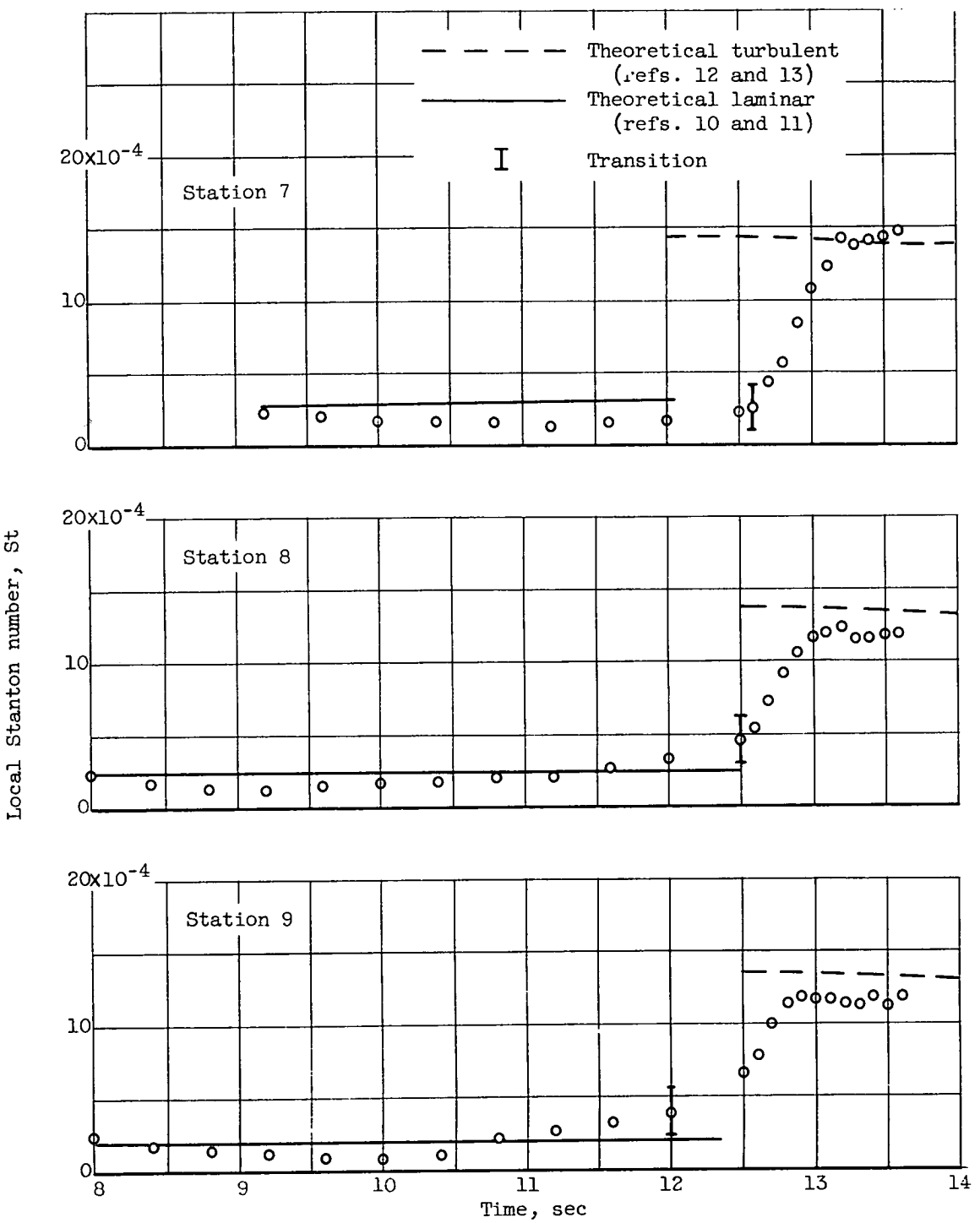

(b) Stations on cylinder and flared afterbody.

Figure 5. - Continued. Time history of local Stanton number for model 3 (50-microin. average roughness).

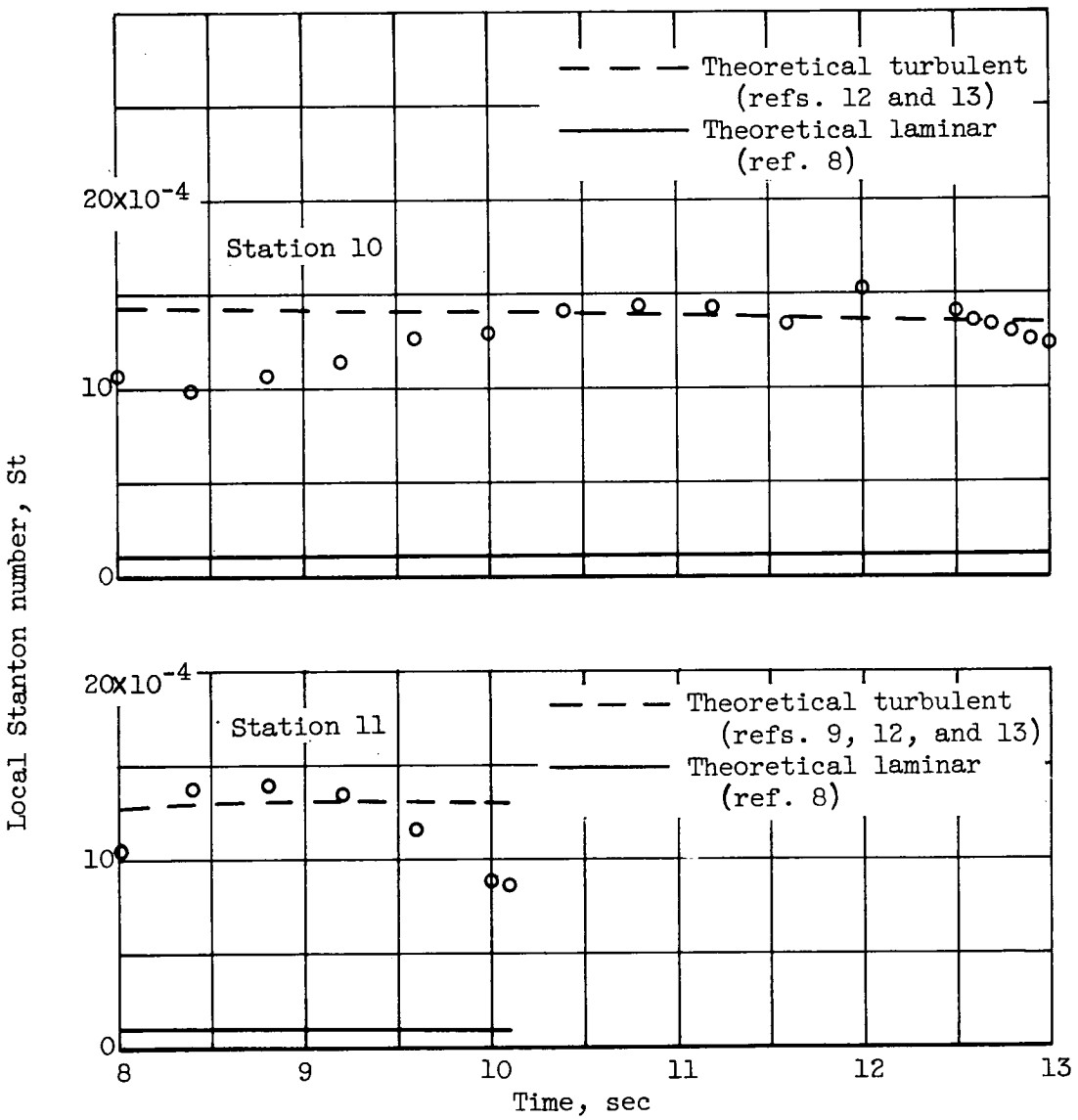

(b) Concluded. Stations on cylinder and flared afterbody.

Figure 5. - Concluded. Time history of local Stanton number for model 3 (50-microin. average roughness).

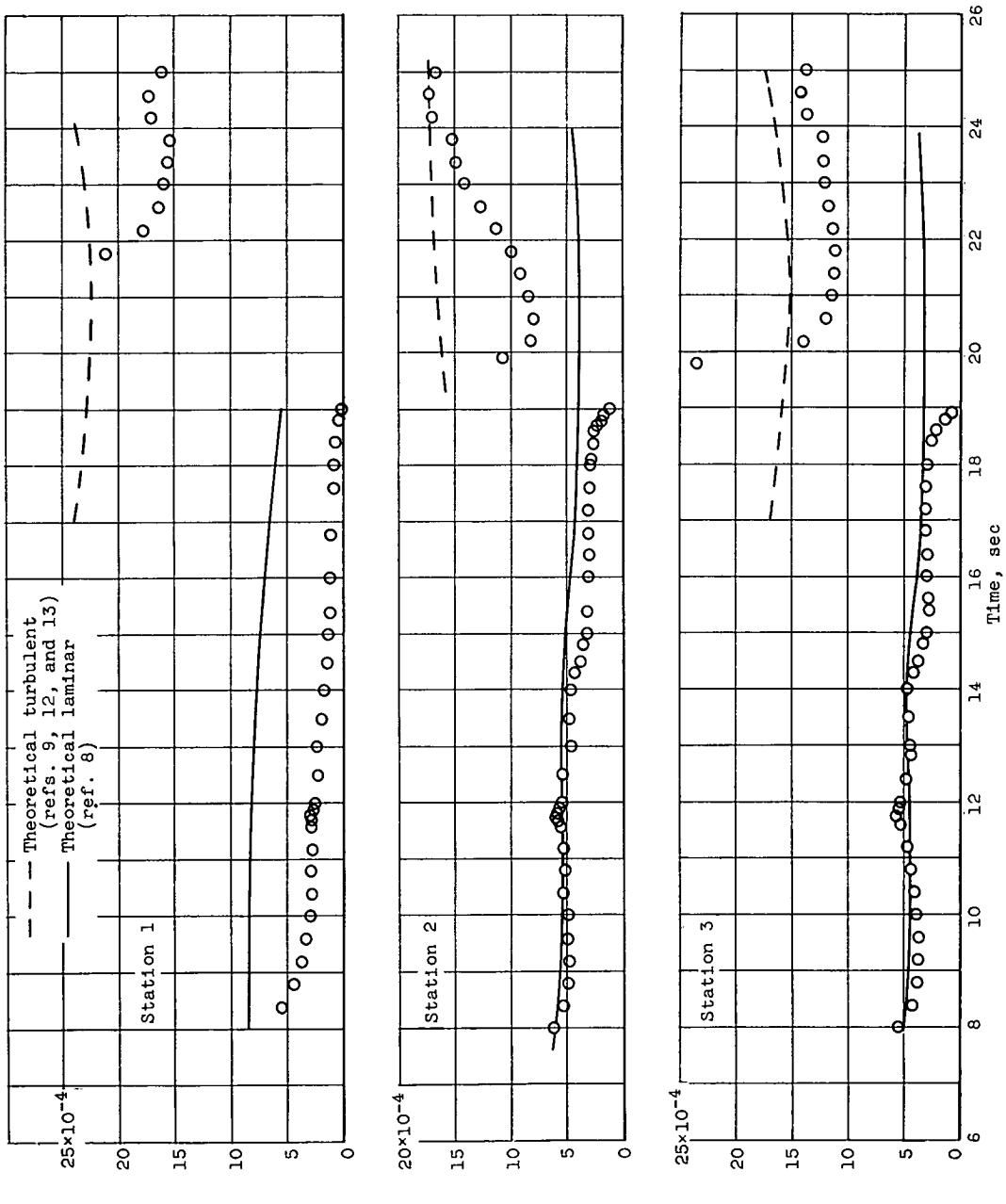

(a) Stations on cone.

Figure 6. - Time history of local Stanton number for model 4 (2-microin. average roughness).

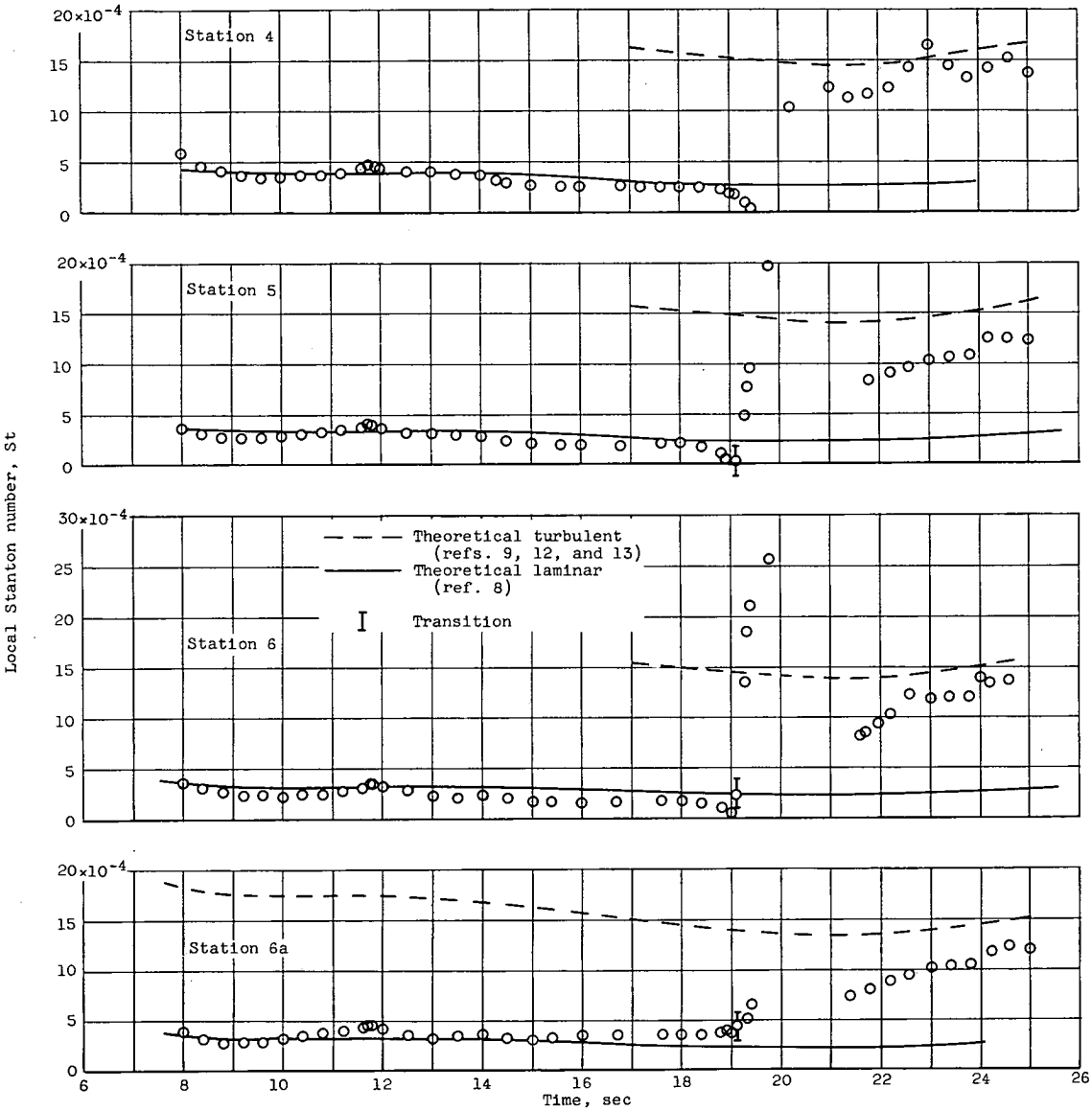

(a) Concluded. Stations on cone.

Figure 6. - Continued. Time history of local Stanton number for model 4 (2-microin. average roughness).

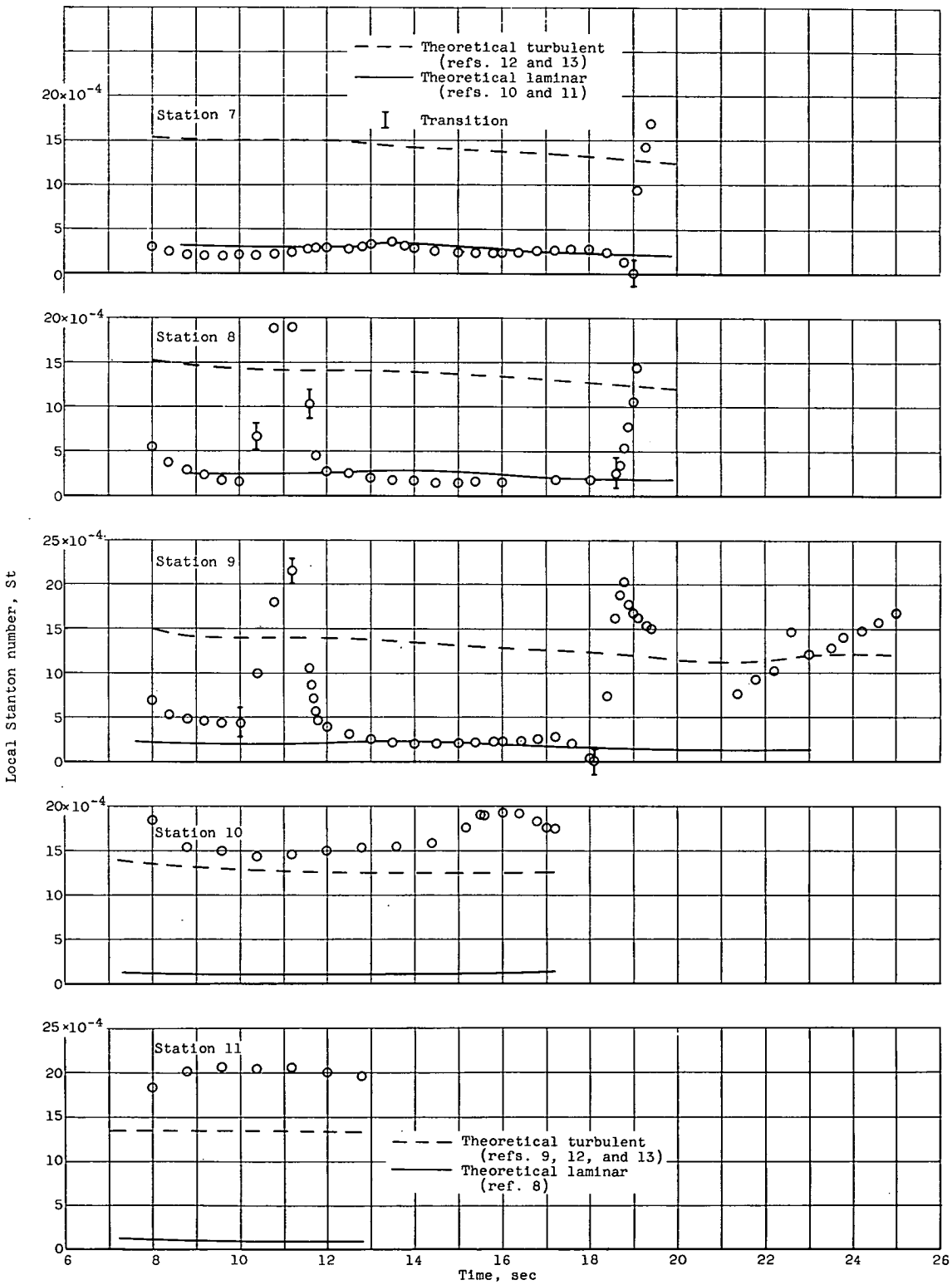

(b) Stations on cylinder and flared afterbody.

Figure 6. - Concluded. Time history of local Stanton number for model 4 (2-microin. average roughness).

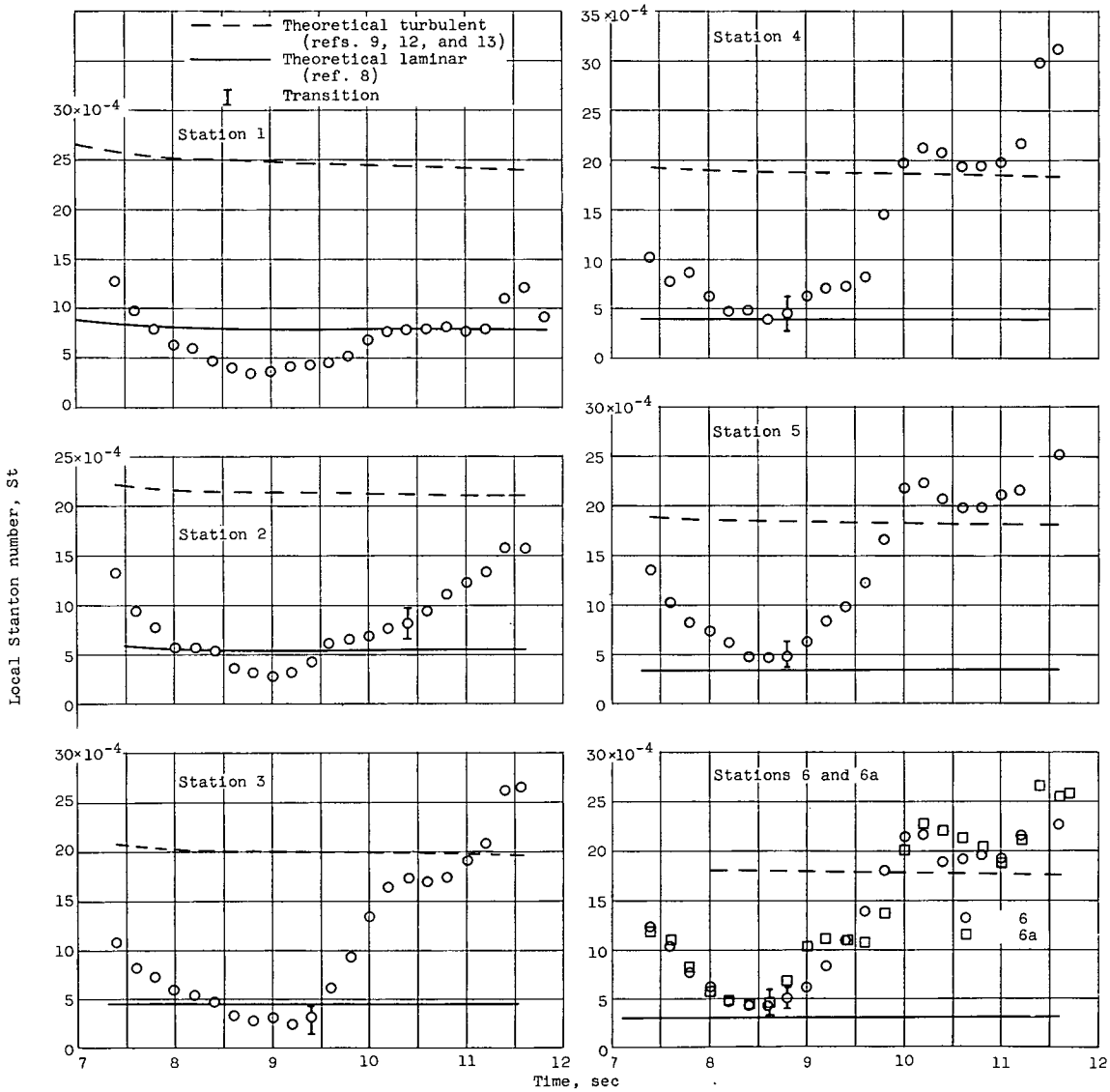

(a) Stations on cone.

Figure 7. - Time history of local Stanton number for model 5 (20-microin. average roughness).

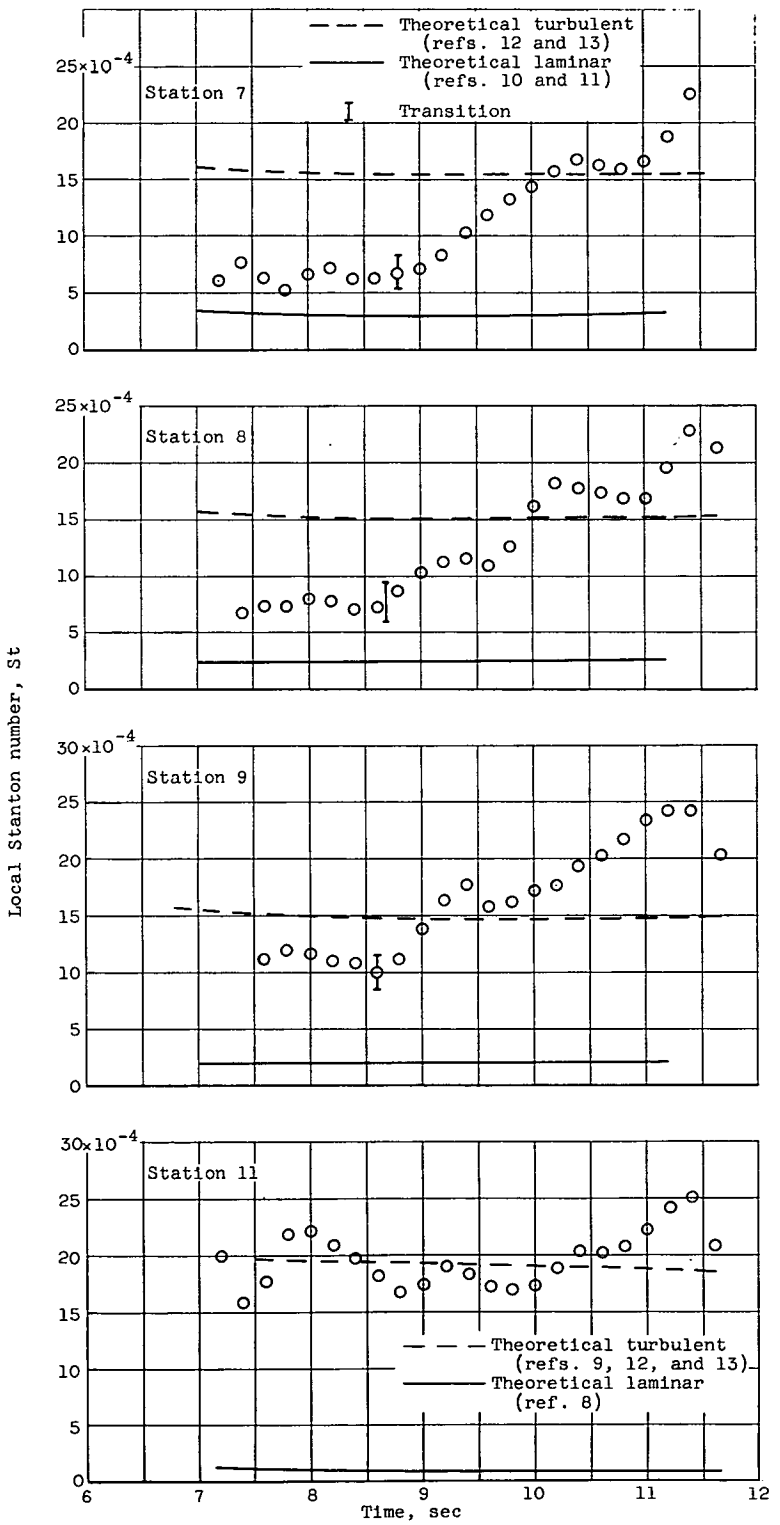

(b) Stations on cylinder and flared afterbody.

Figure 7. - Concluded. Time history of local Stanton number for model 5 (20-microin. average roughness).

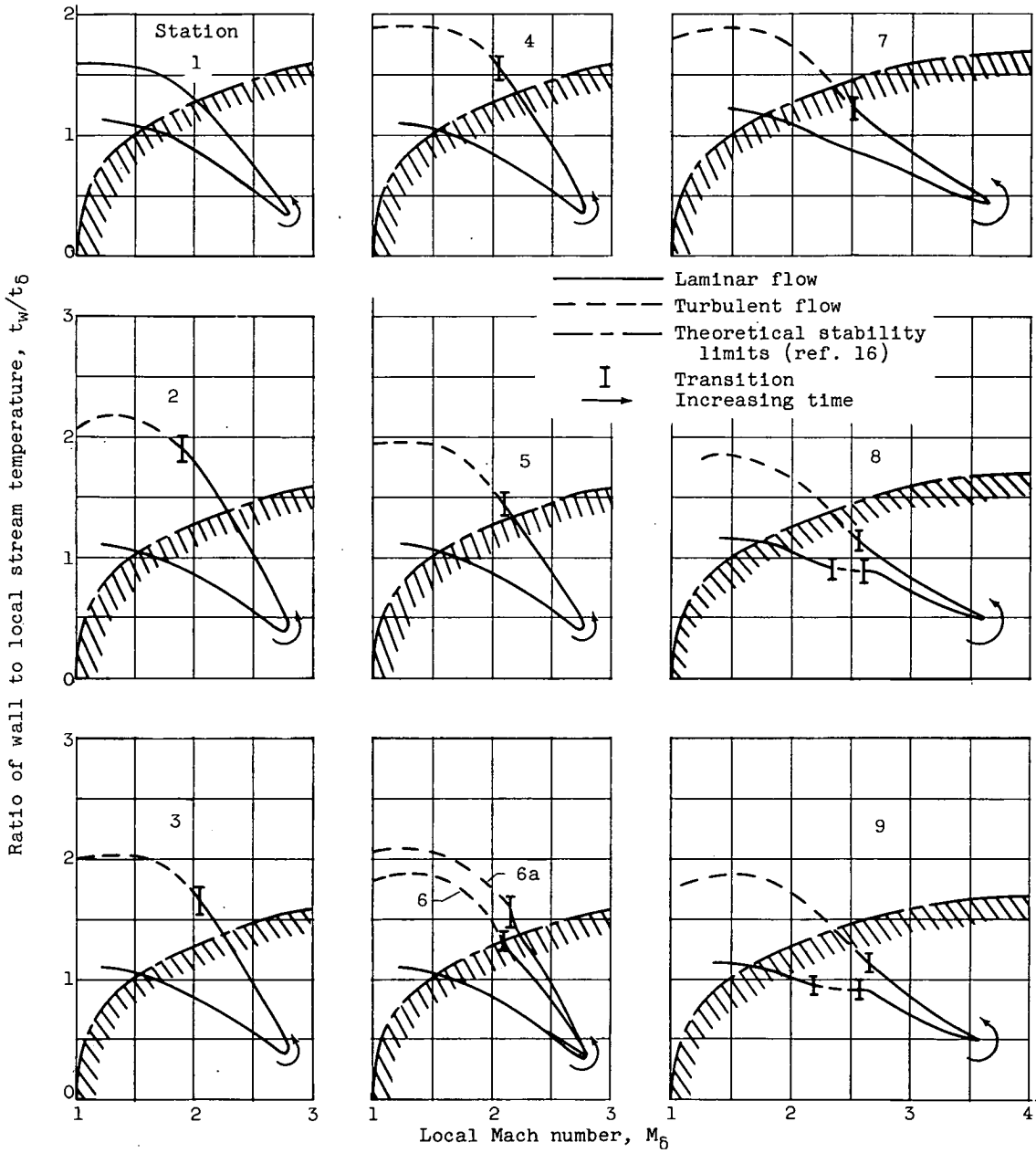

(a) Stations on cone. (b) Stations on cylinder.

Figure 8. - Variation of local temperature ratio with local Mach number for model 4 (2-microin. average roughness).

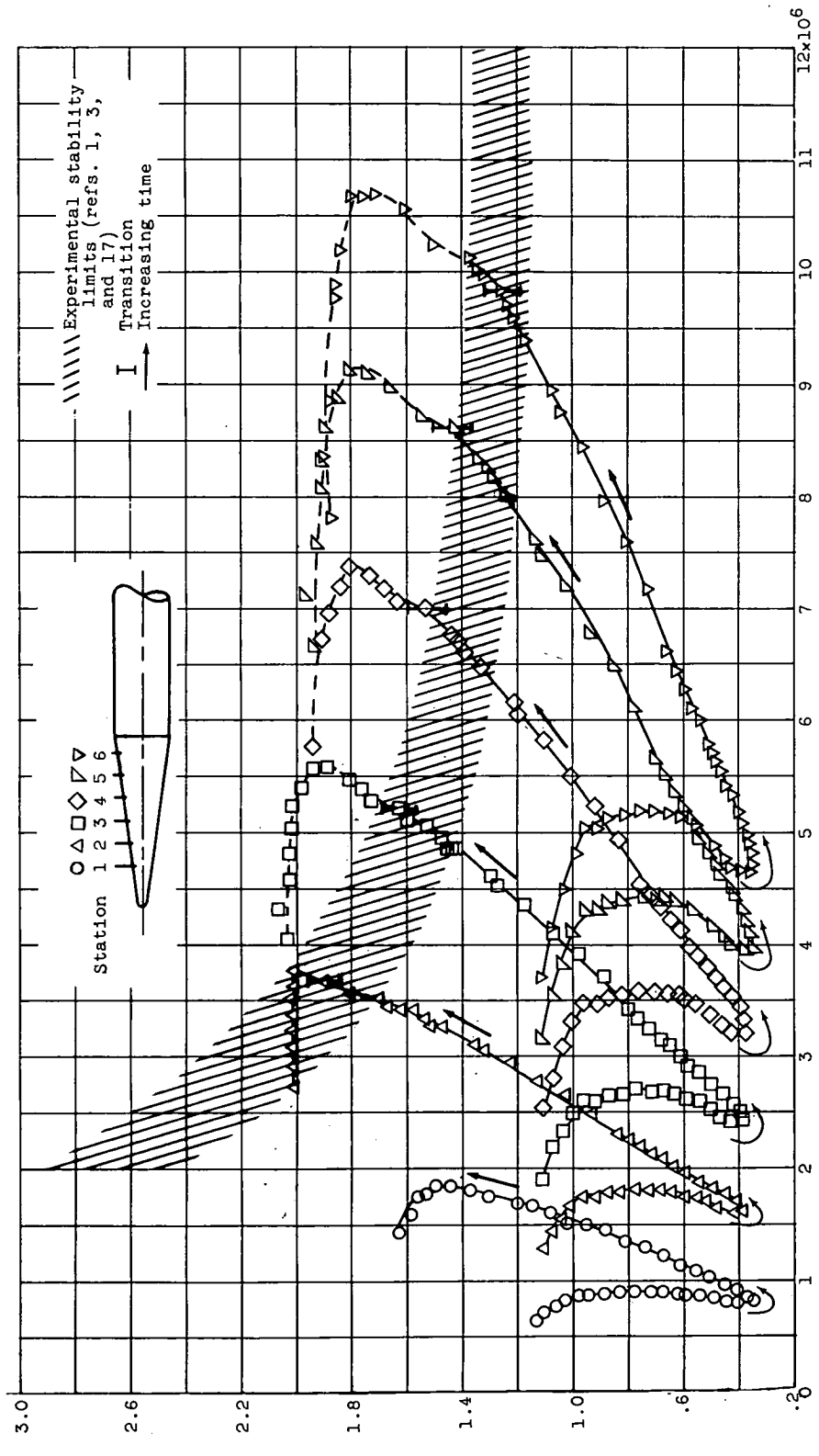

(a) Stations on cone.

Figure 9. - Variation of local temperature ratio with local Reynolds number for model 4 (2-microin. average roughness).

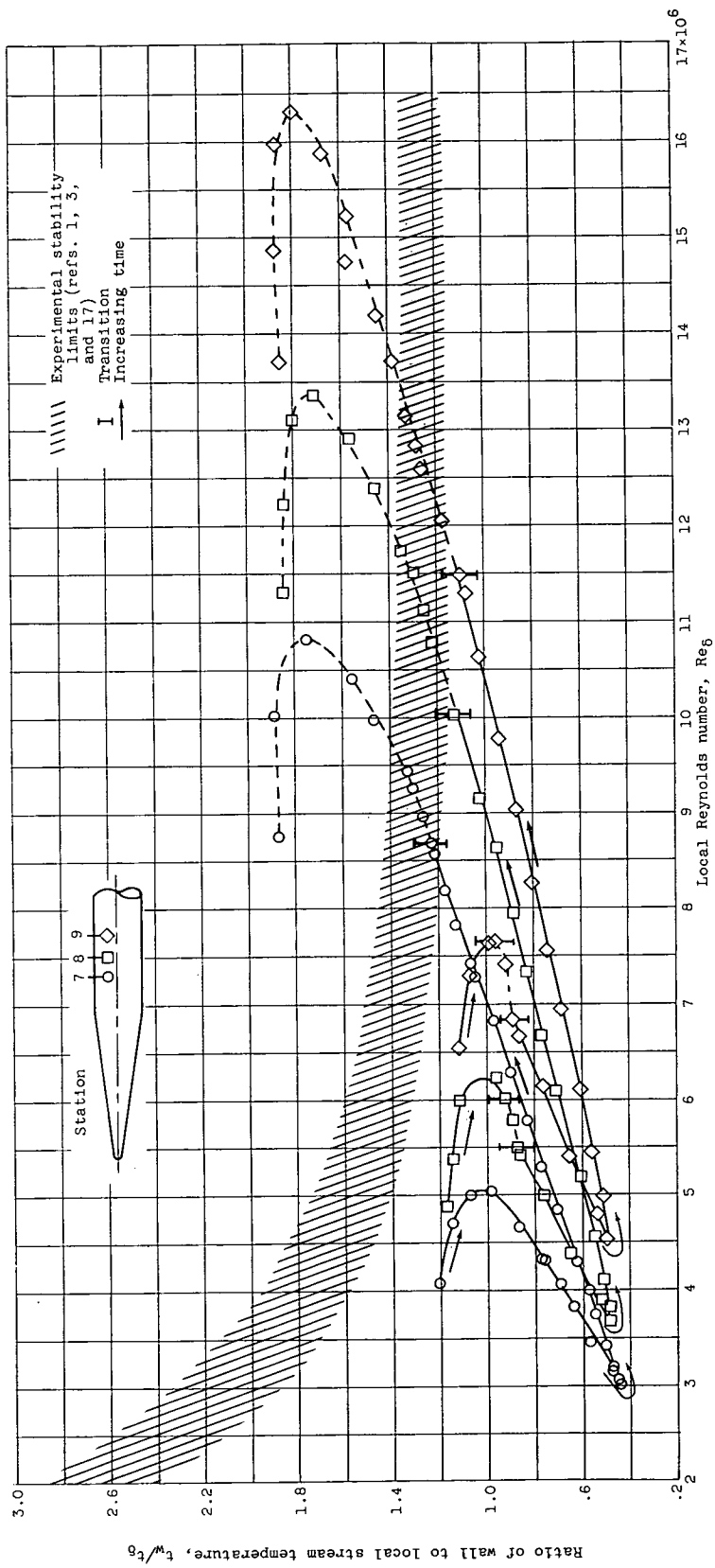

(b) Stations on cylinder.

Figure 9. - Concluded. Variation of local temperature ratio with local Reynolds number for model 4 (2-microin. average roughness).

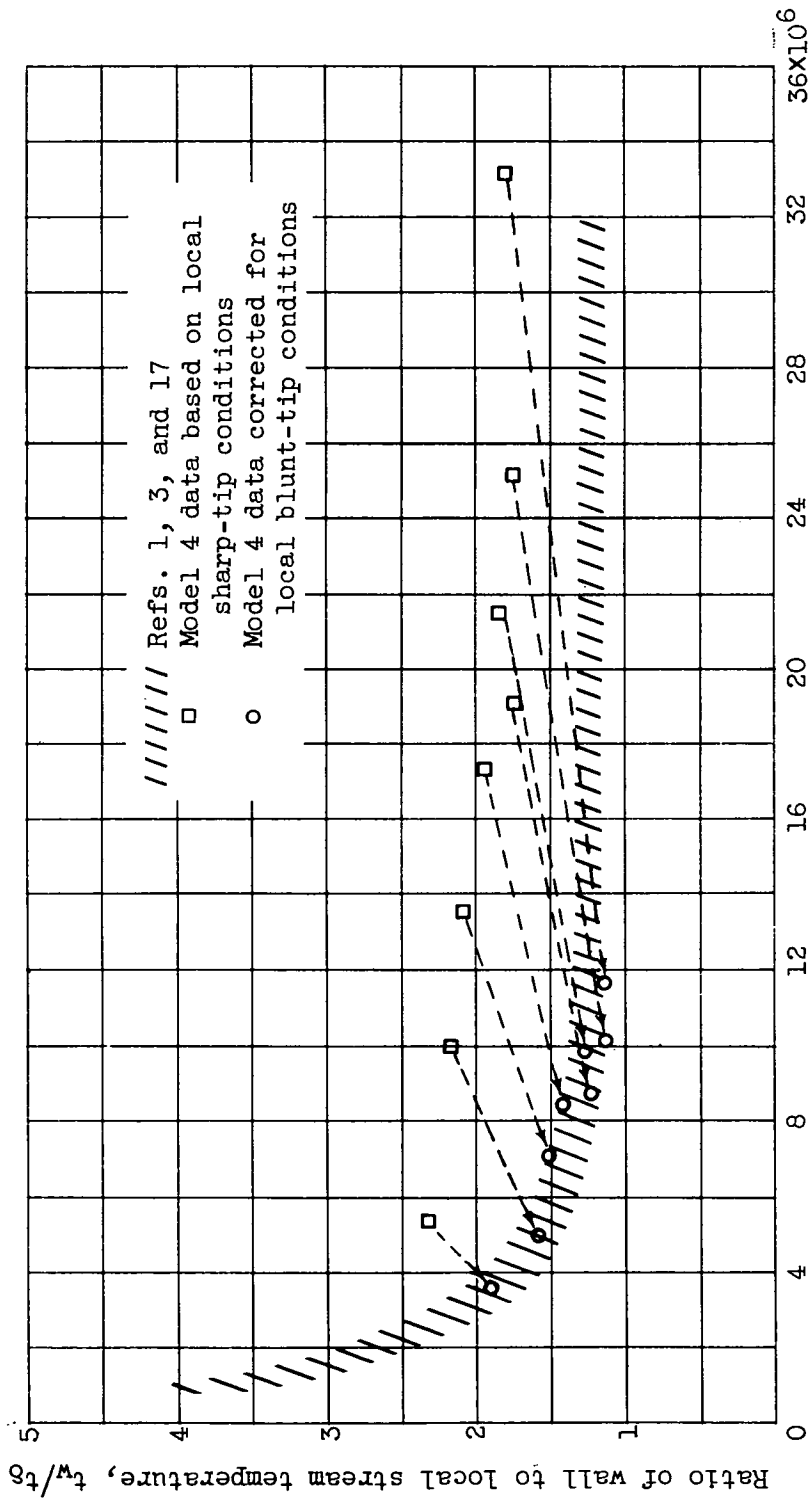

Figure 10. - Comparison of transition Reynolds numbers and local temperature ratios of model 4 (2-microin. average roughness) with data from other investigations.

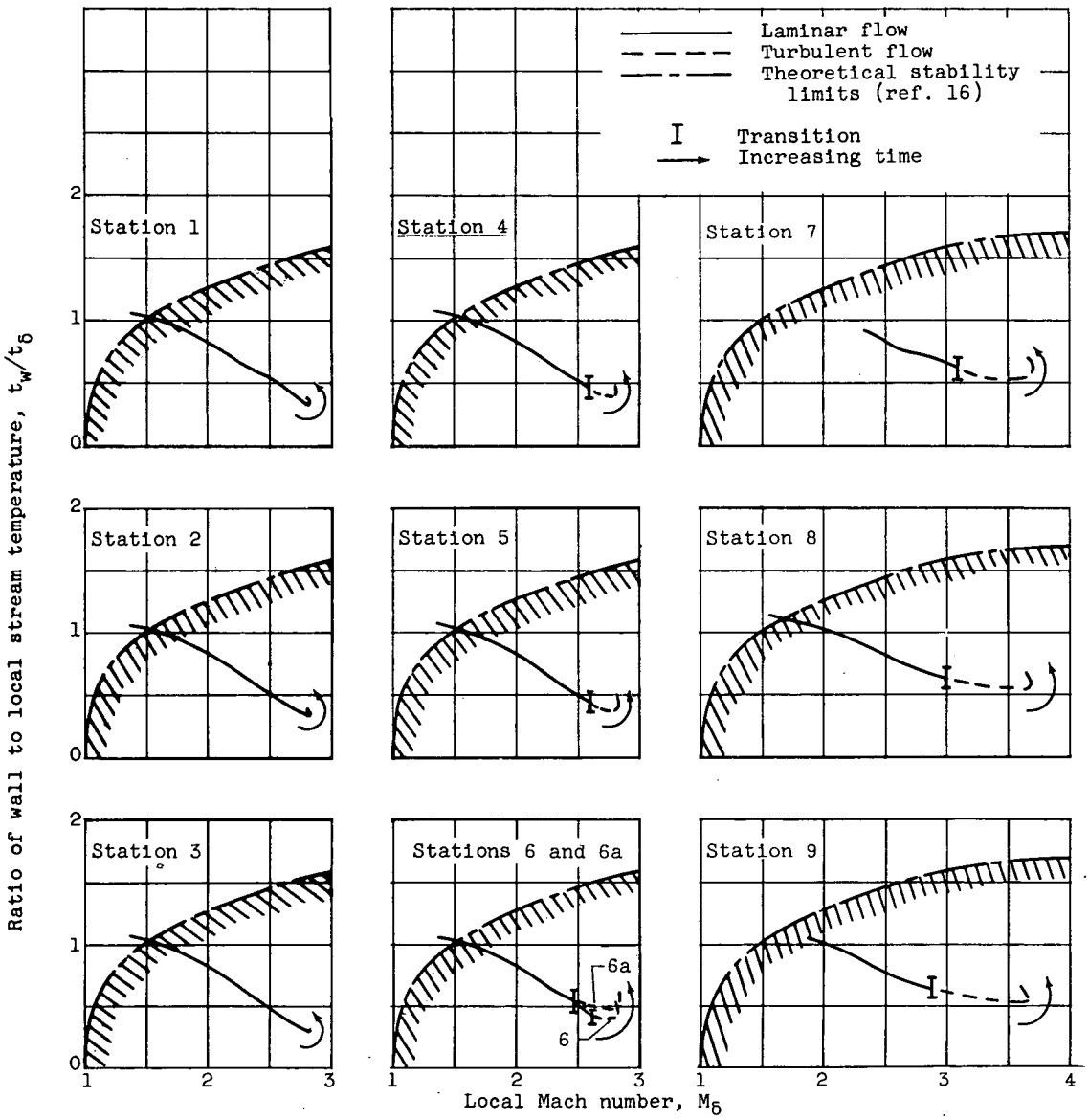

(a) Stations on cone. (b) Stations on cylinder.

Figure 11. - Variation of local temperature ratio with local Mach number for model 3 (50-microin. average roughness).

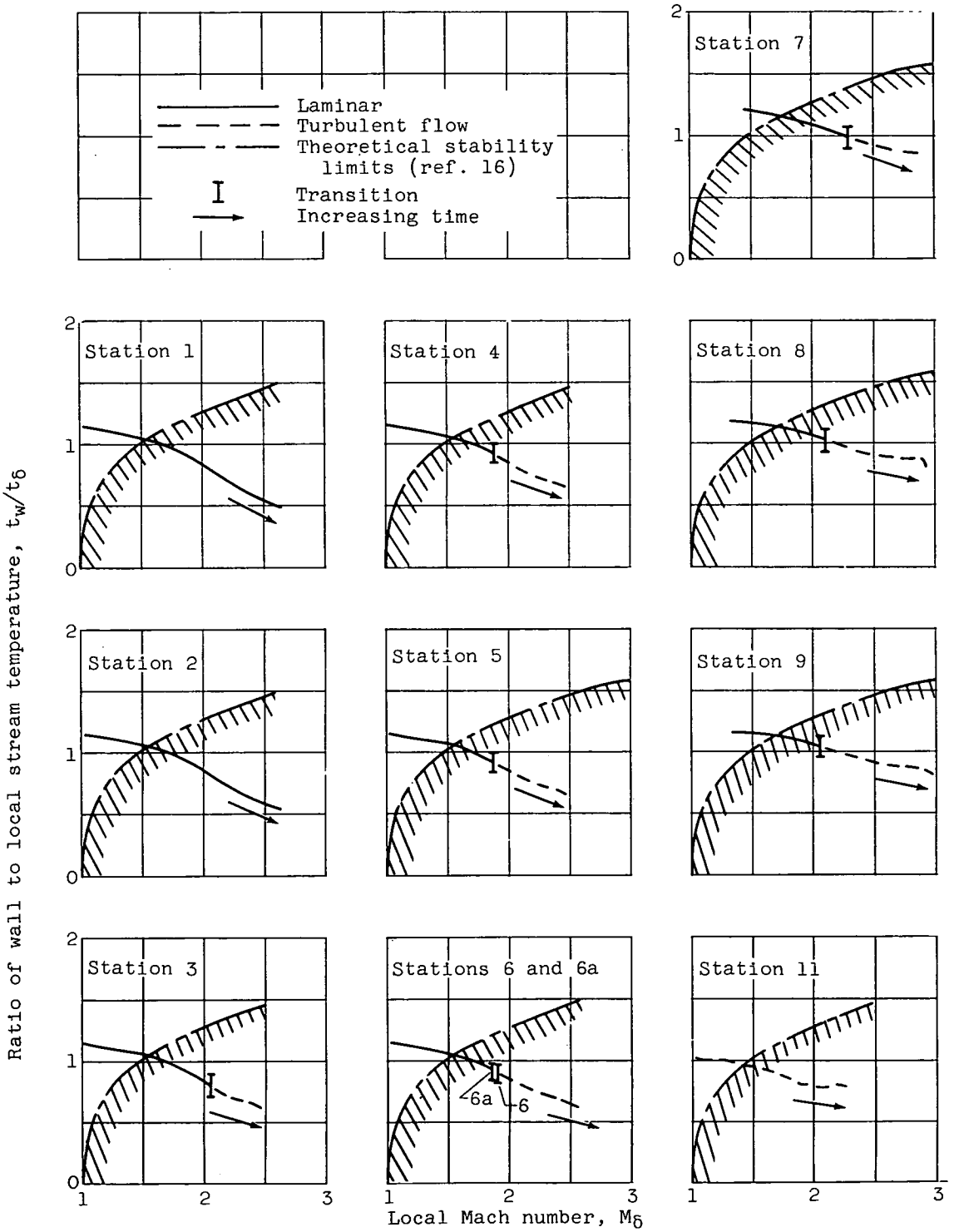

(a) Stations on cone.

(b) Stations on cylinder and flared afterbody.

Figure 12. - Variation of local temperature ratio with local Mach number for model 5 (20-microin. average roughness).

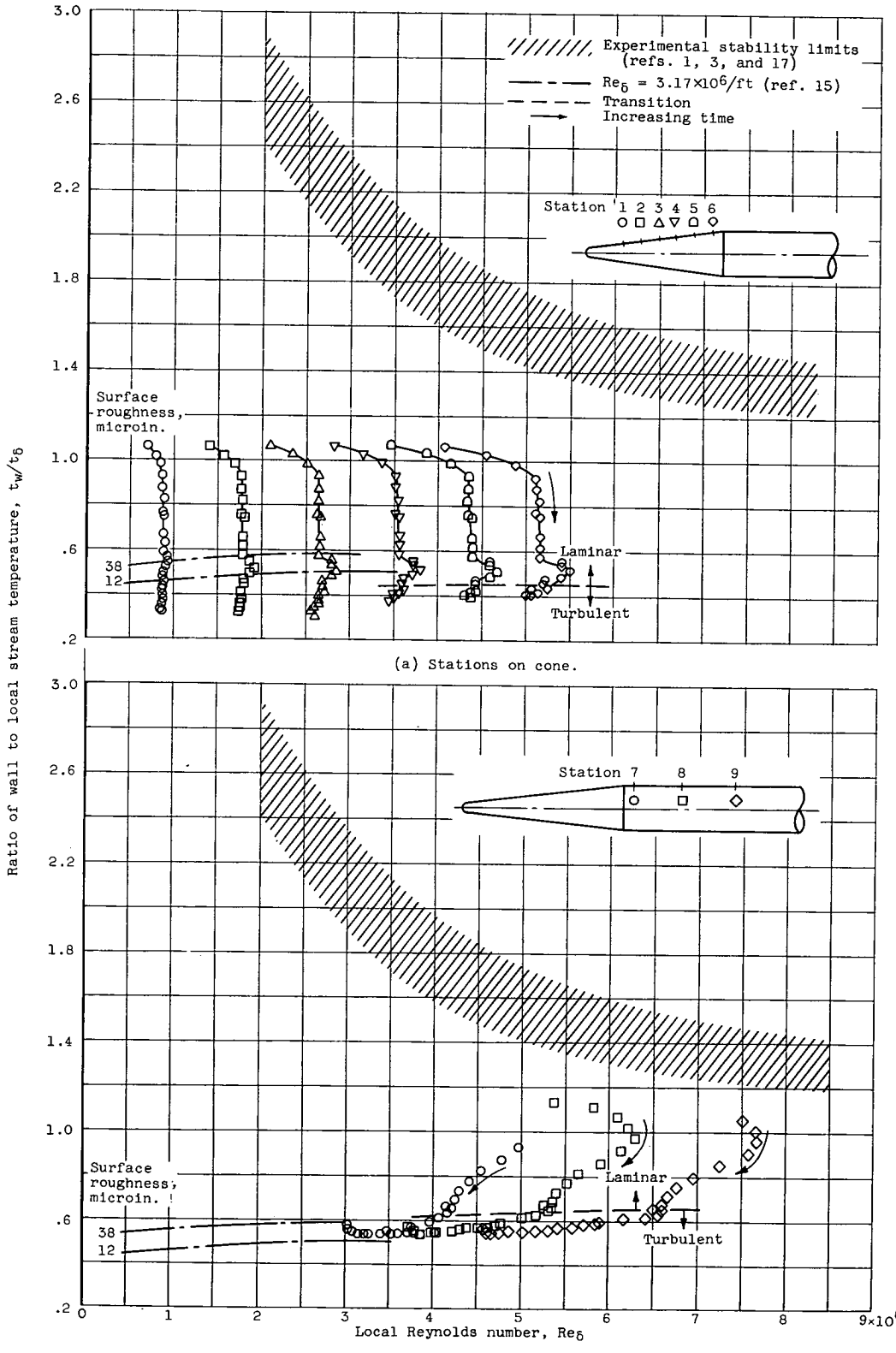

Figure 13. - Variation of local temperature ratio with local Reynolds number for model 3 (50-microin. average roughness).

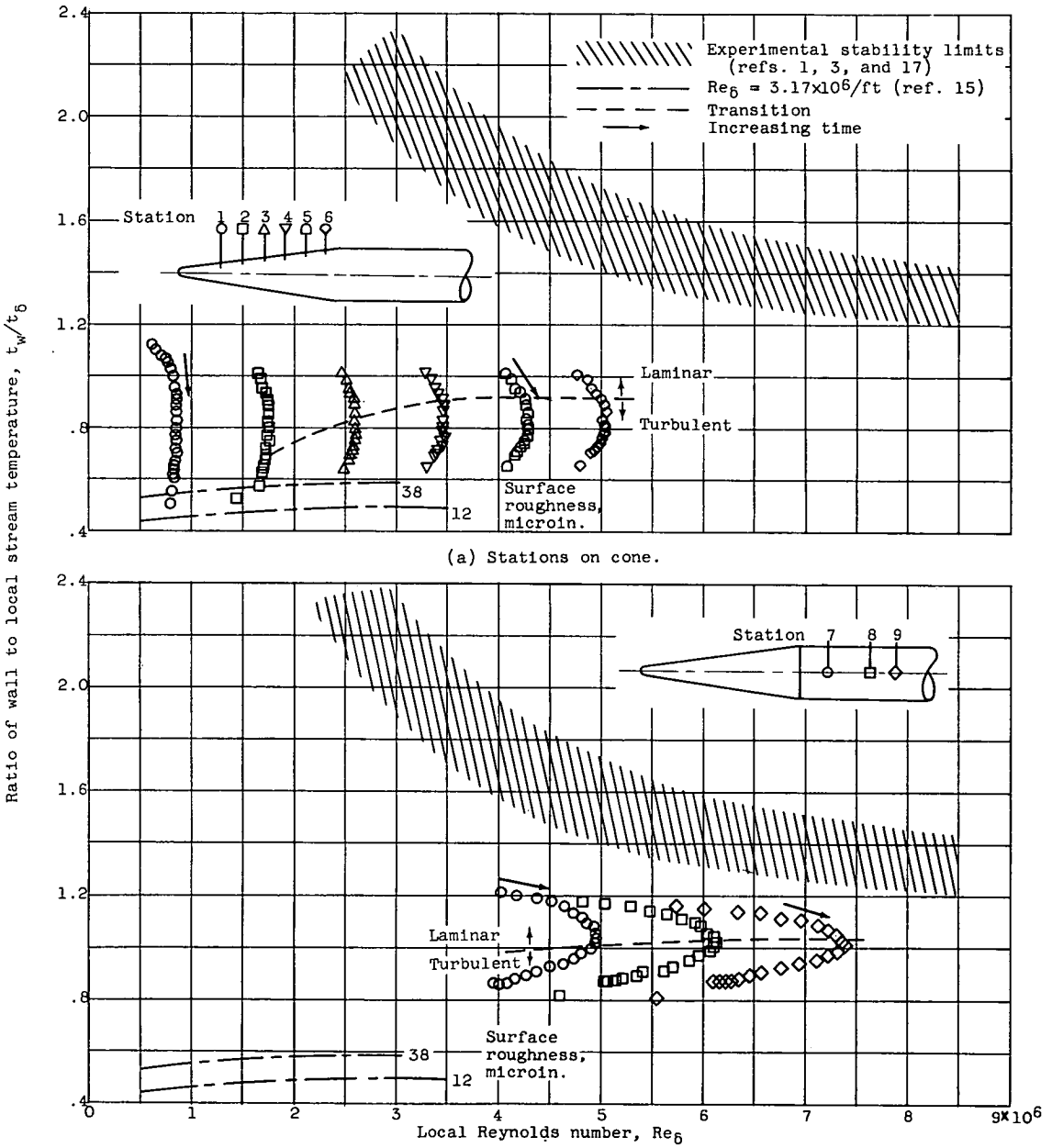

(a) Stations on cone.

(b) Stations on cylinder.

Figure 14. - Variation of local temperature ratio with local Reynolds number for model 5 (20-microin. average roughness).

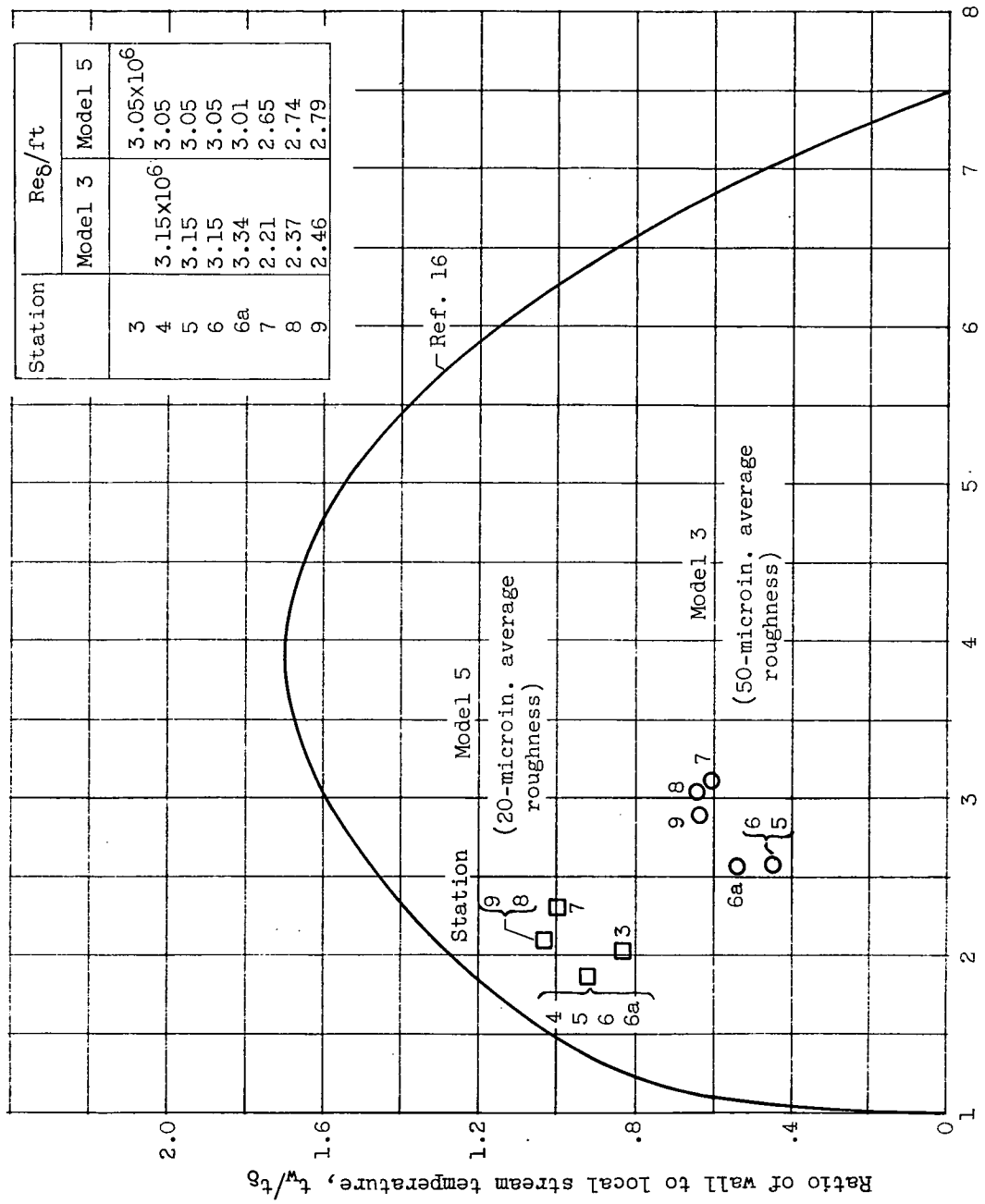

Figure 15. - Summary of transition data of models 3 and 5.

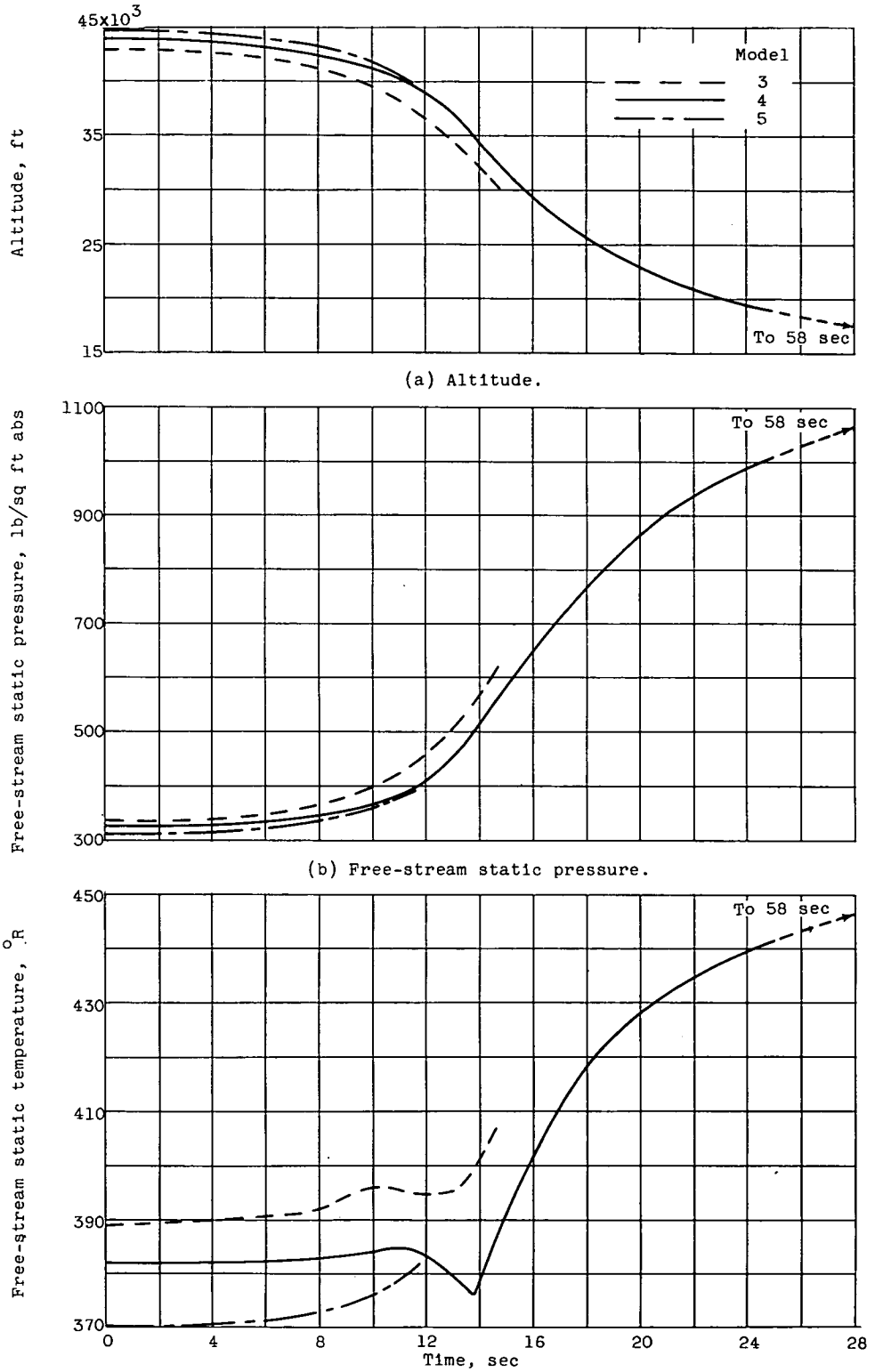

(a) Altitude.

(b) Free-stream static pressure.

(c) Free-stream static temperature.

Figure 16. - Atmospheric conditions during flight for models 3, 4, and 5.

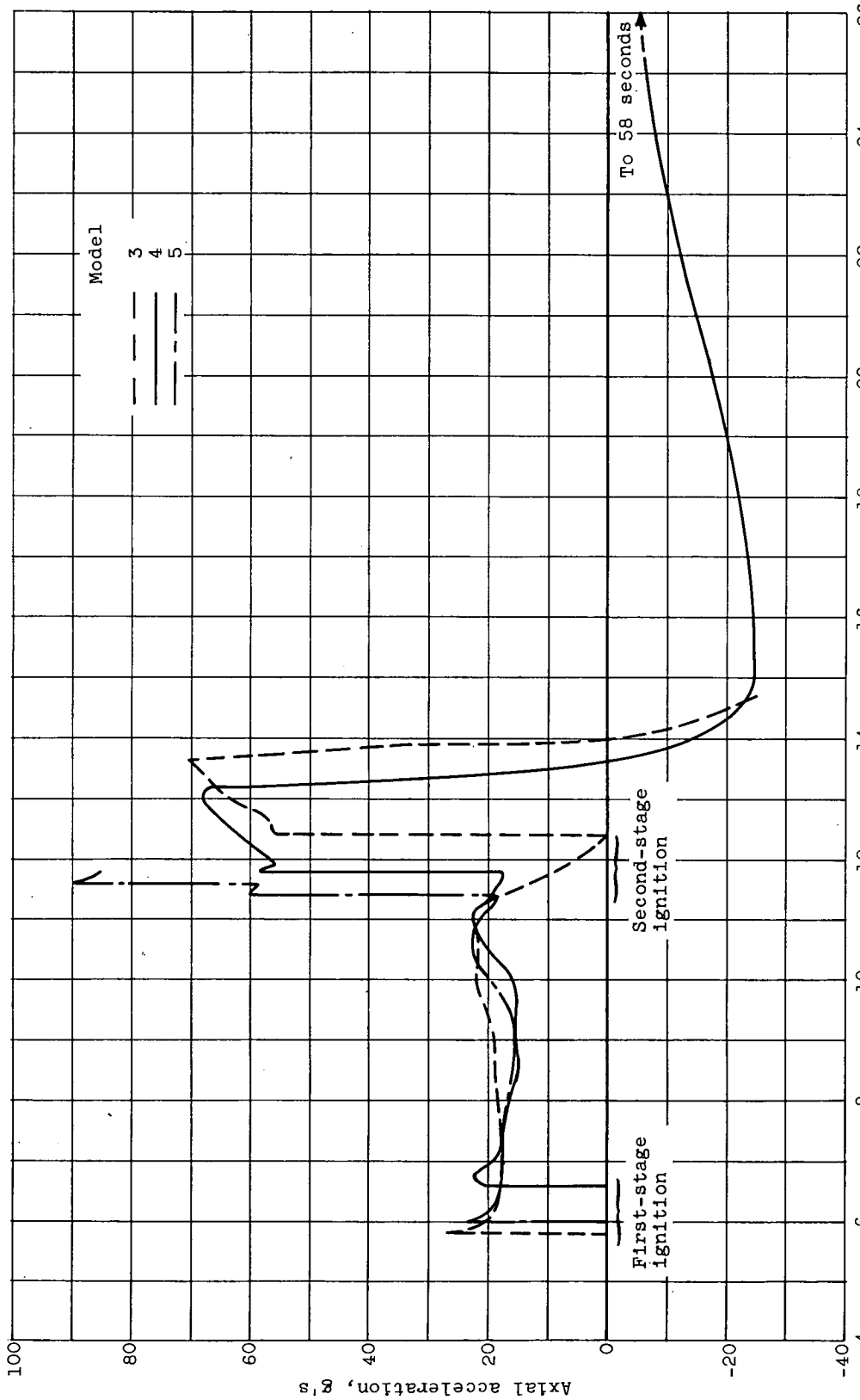

Figure 17. - Time history of accelerations for models 3, 4, and 5.

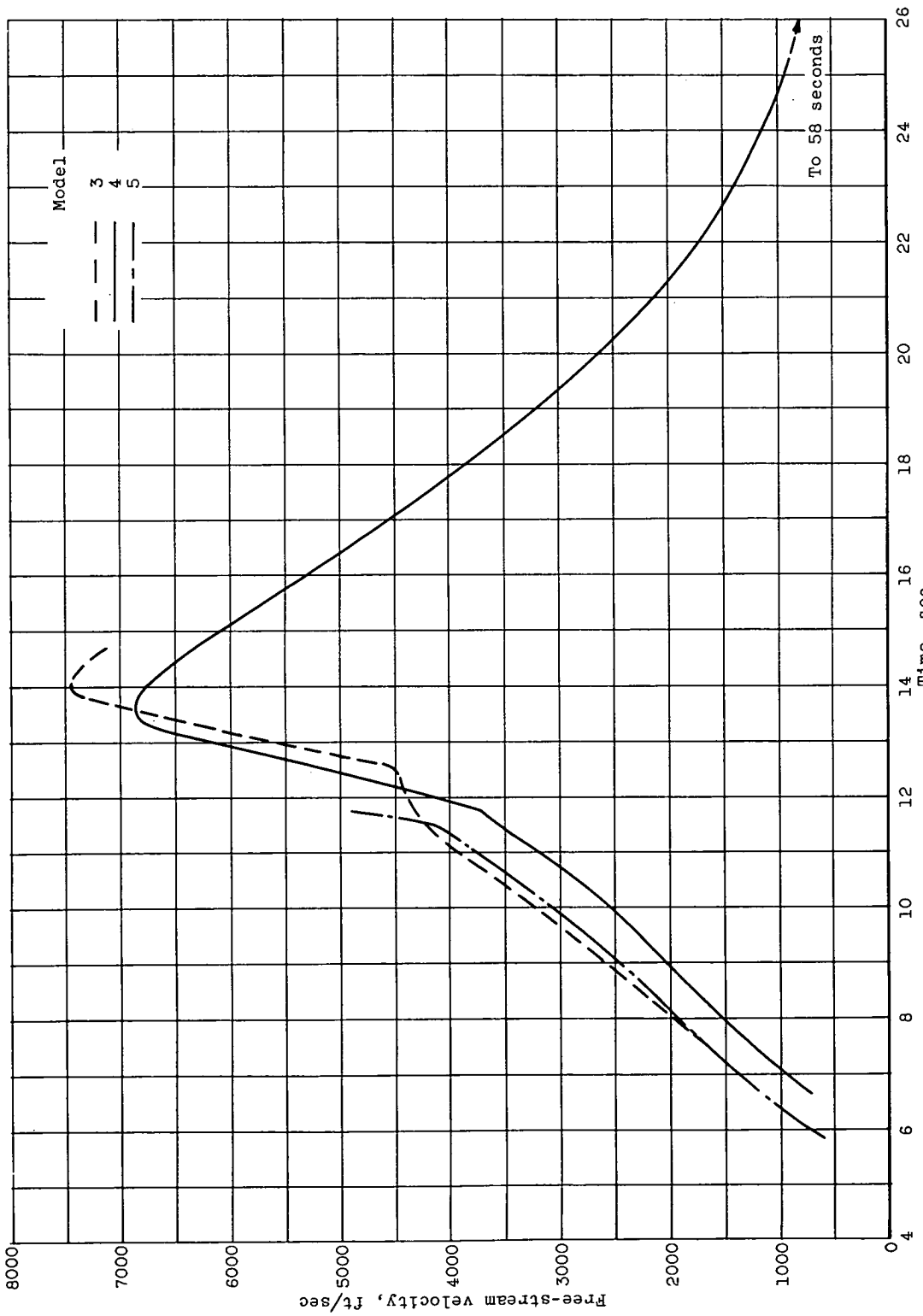

Figure 18. - Time history of free-stream velocity for models 3, 4, and 5.

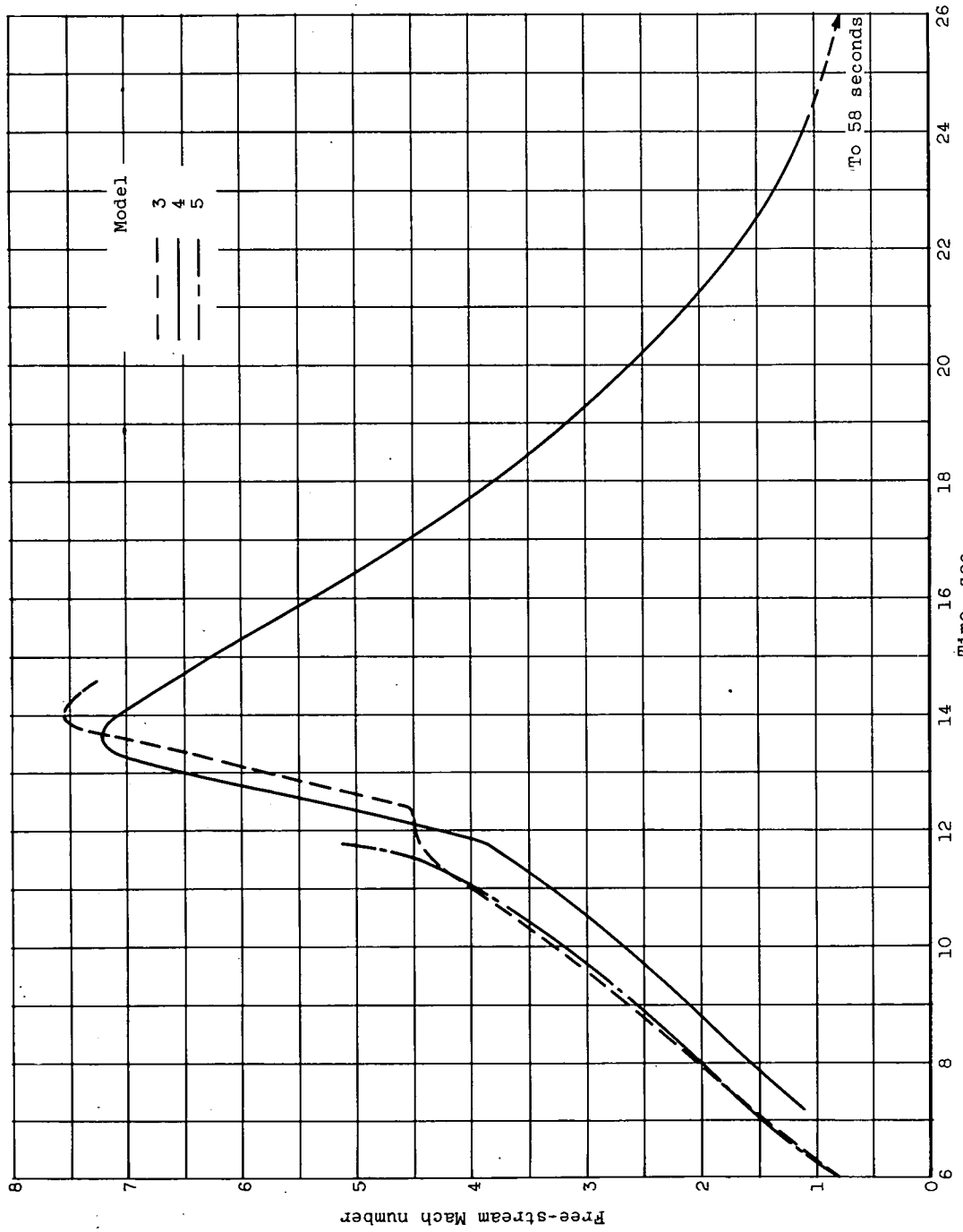

Figure 19. - Time history of free-stream Mach number for models 3, 4, and 5.

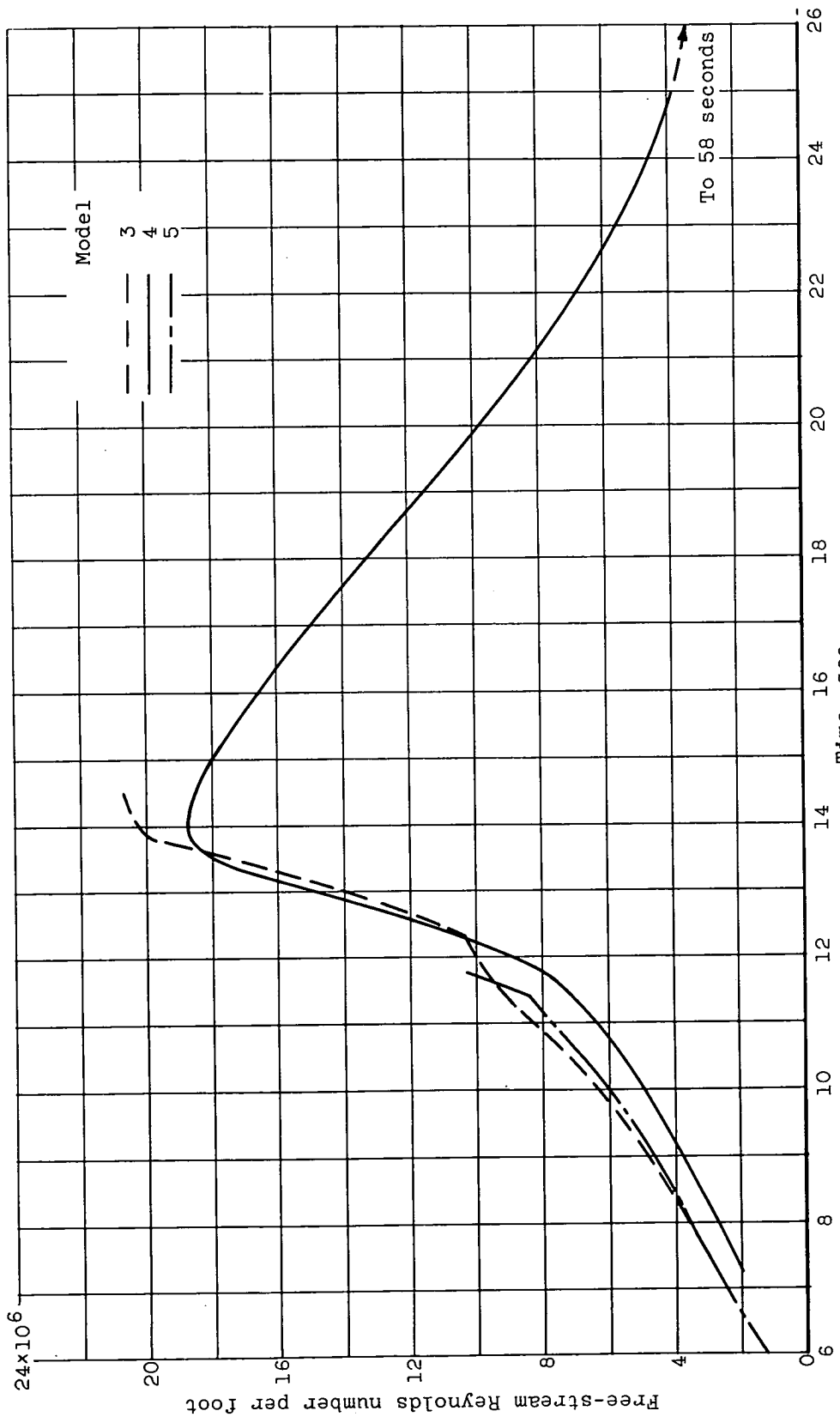

Figure 20. - Time history of free-stream Reynolds number per foot for models 3, 4, and 5.

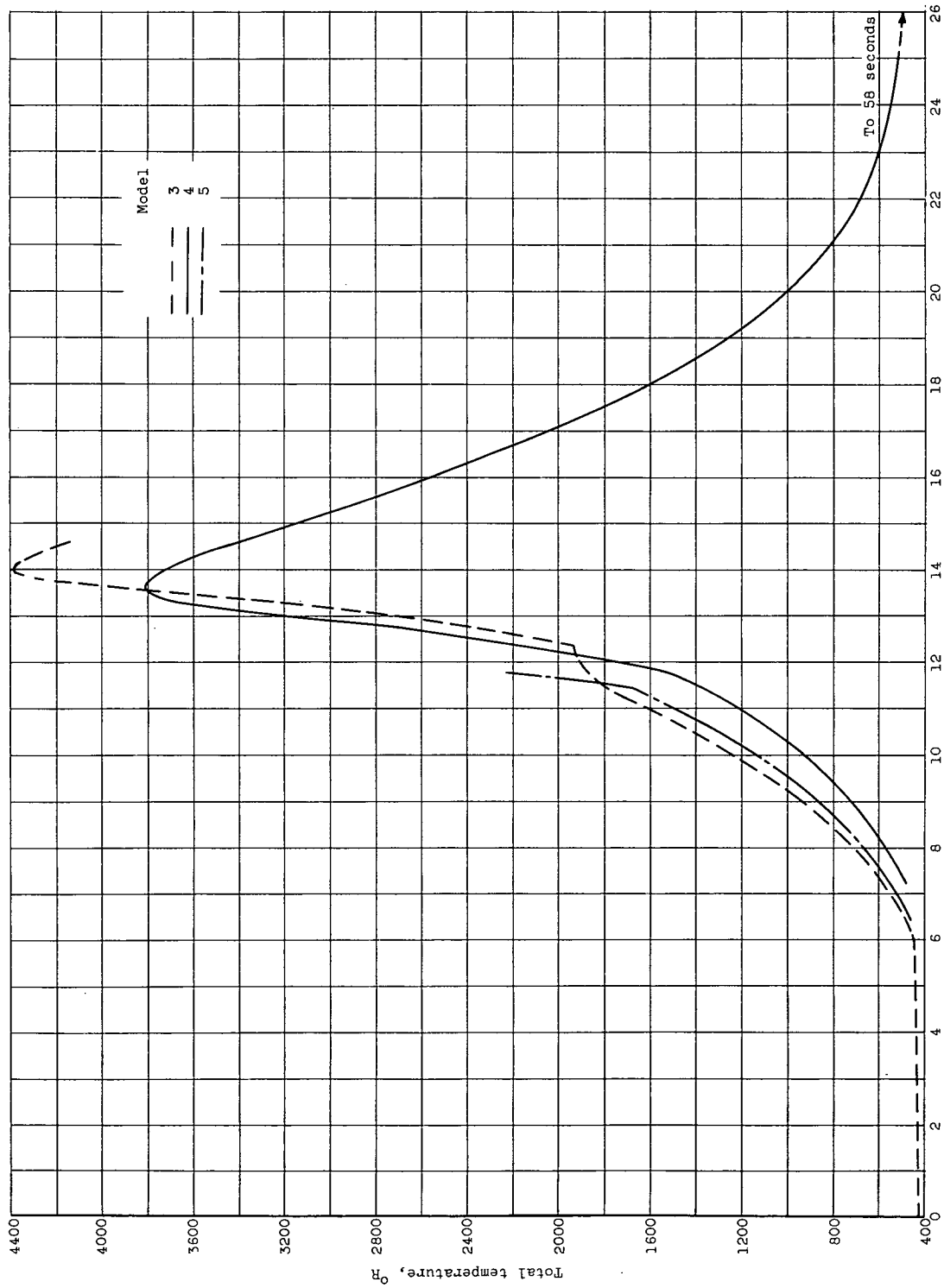

Figure 21. - Time history of free-stream total temperature for models 3, 4, and 5.

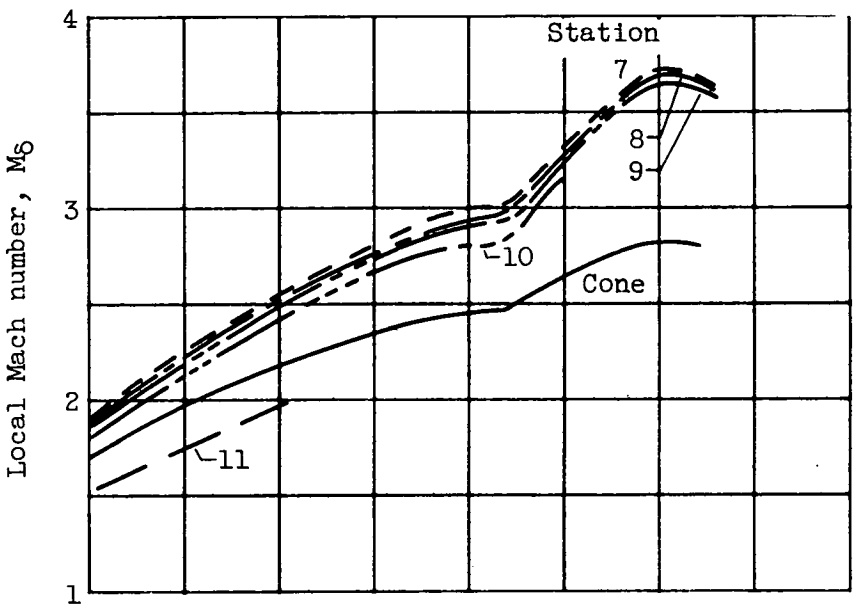

(a) Mach number.

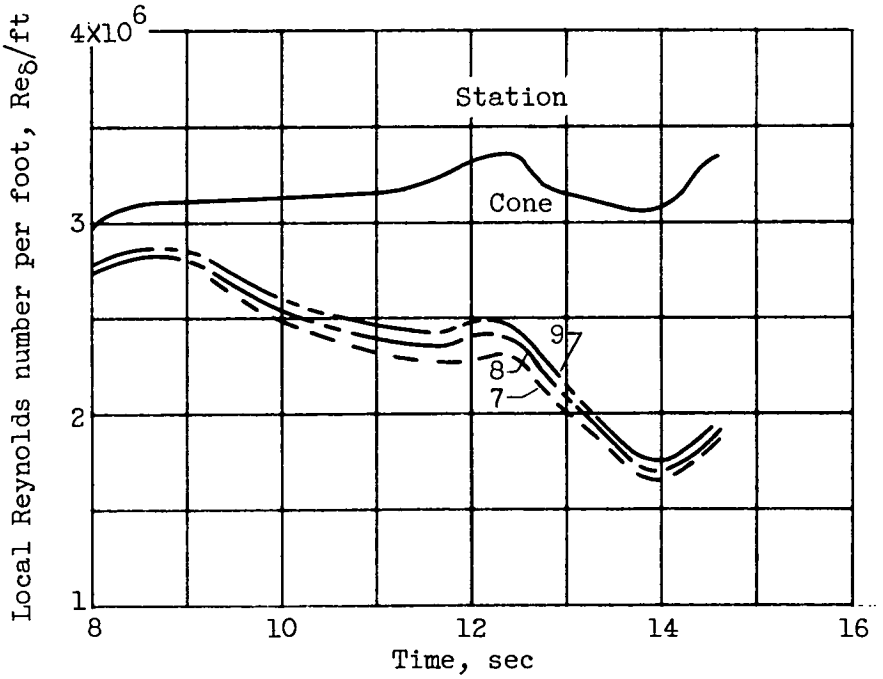

(b) Reynolds number per foot.

Figure 22. - Time history of local Mach number and Reynolds number per foot for model 3 (50-microin. average roughness).

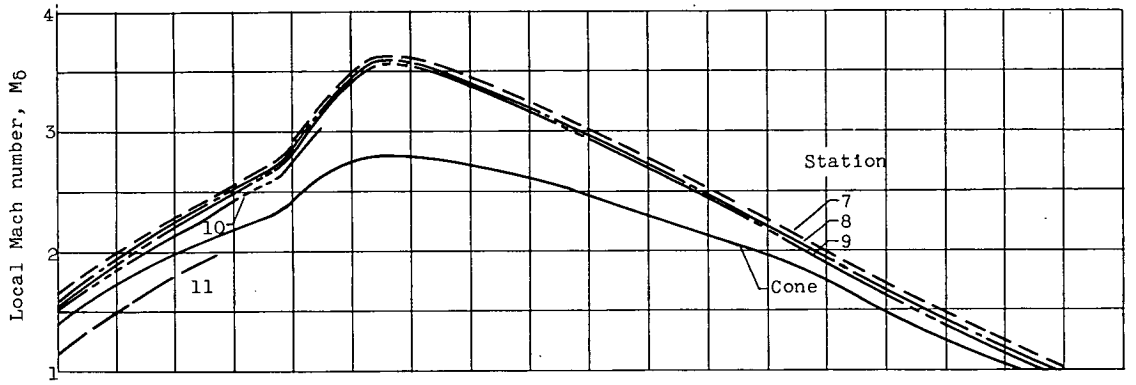

(a) Mach number.

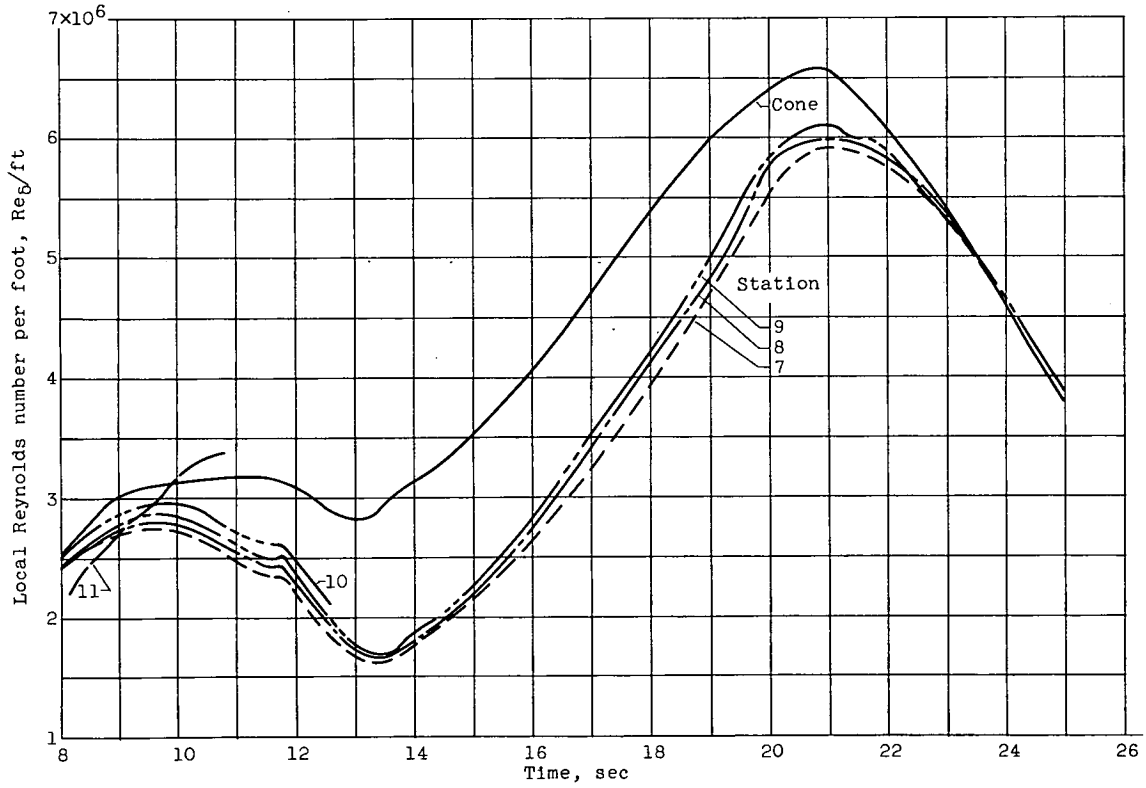

(b) Reynolds number per foot.

Figure 23. - Time history of local Mach number and Reynolds number per foot for model 4 (2-microin. average roughness).

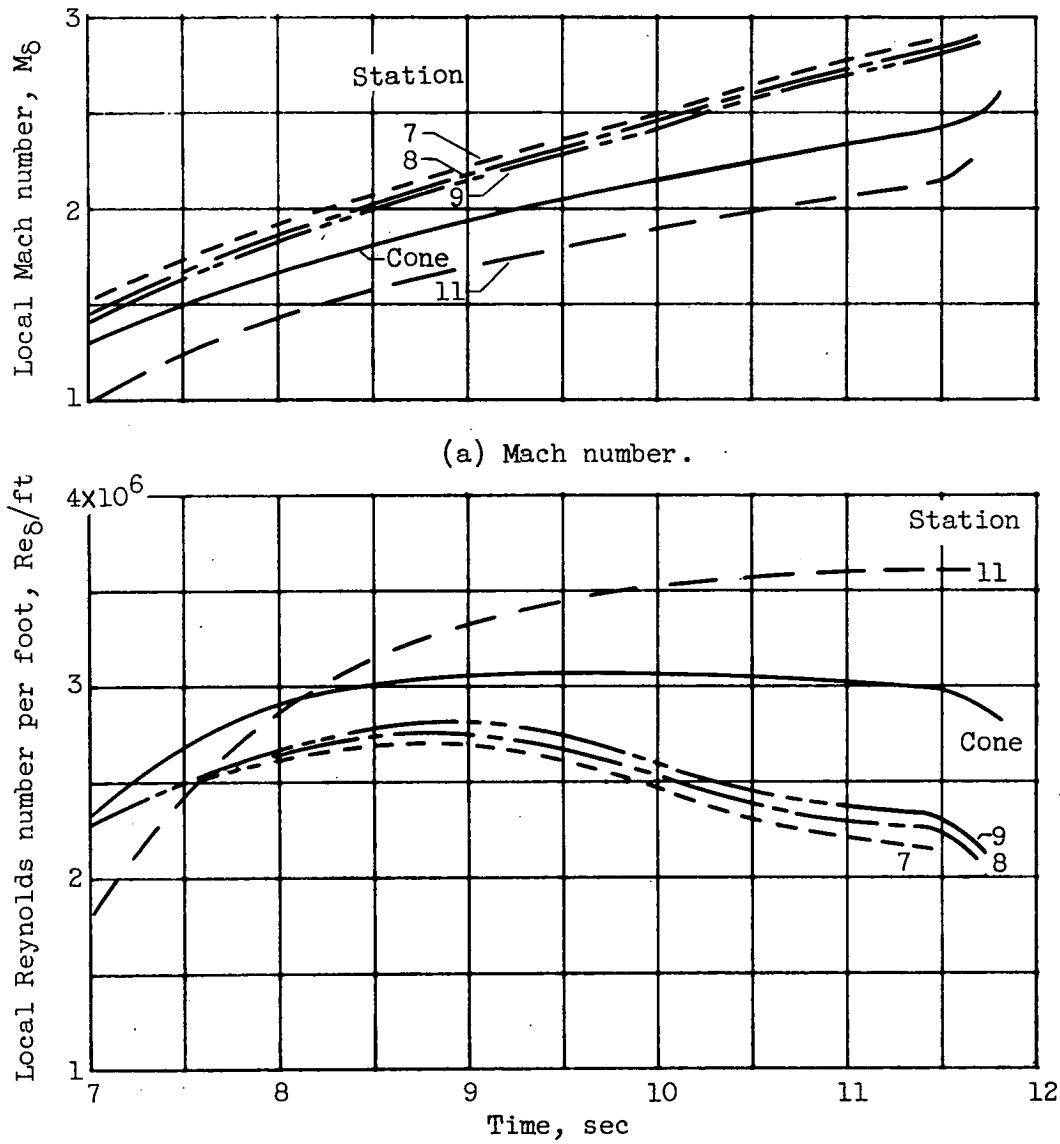

(a) Mach number.

(b) Reynolds number per foot.

Figure 24. - Time history of local Mach number and Reynolds number per foot for model 5 (20-microin. average roughness).

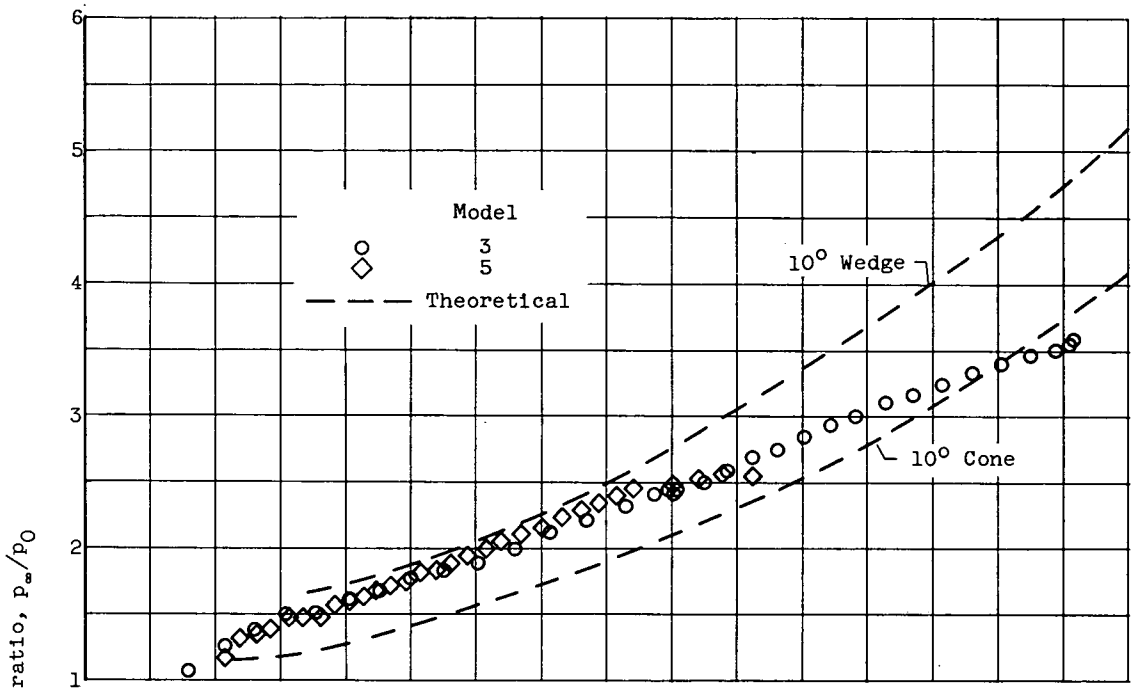

(a) Models 3 and 5.

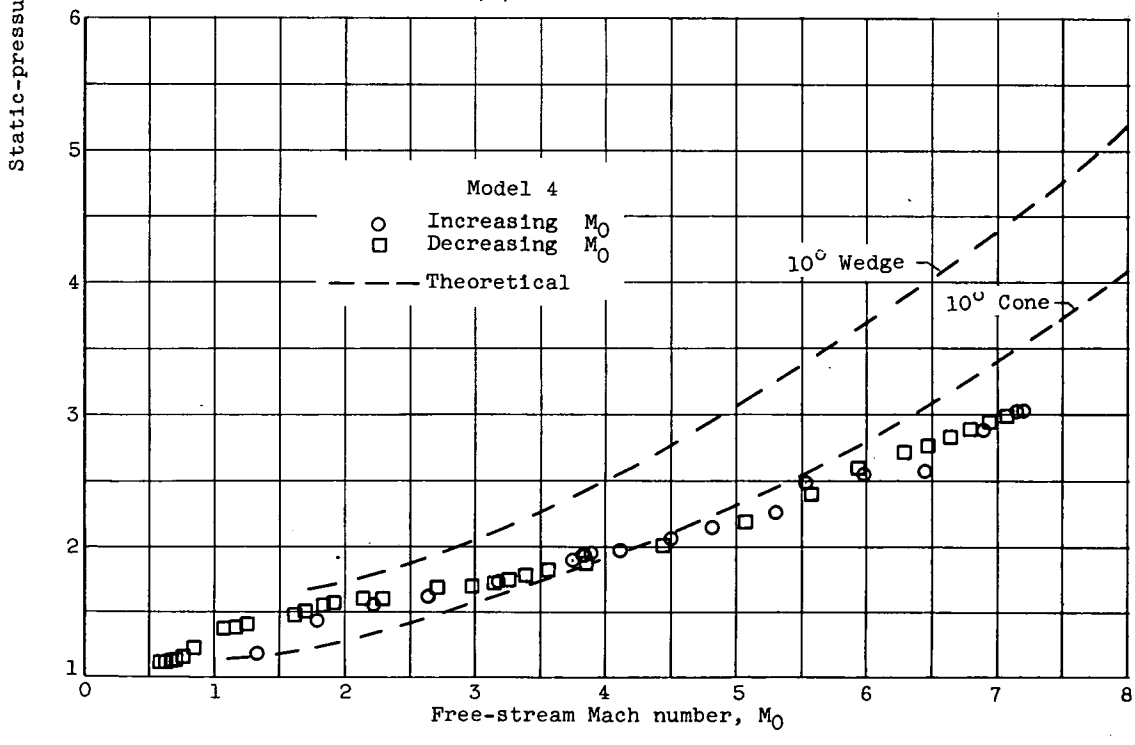

(b) Model 4.

Figure 25. - Variation of static-pressure ratio on flared afterbody with free-stream Mach number.

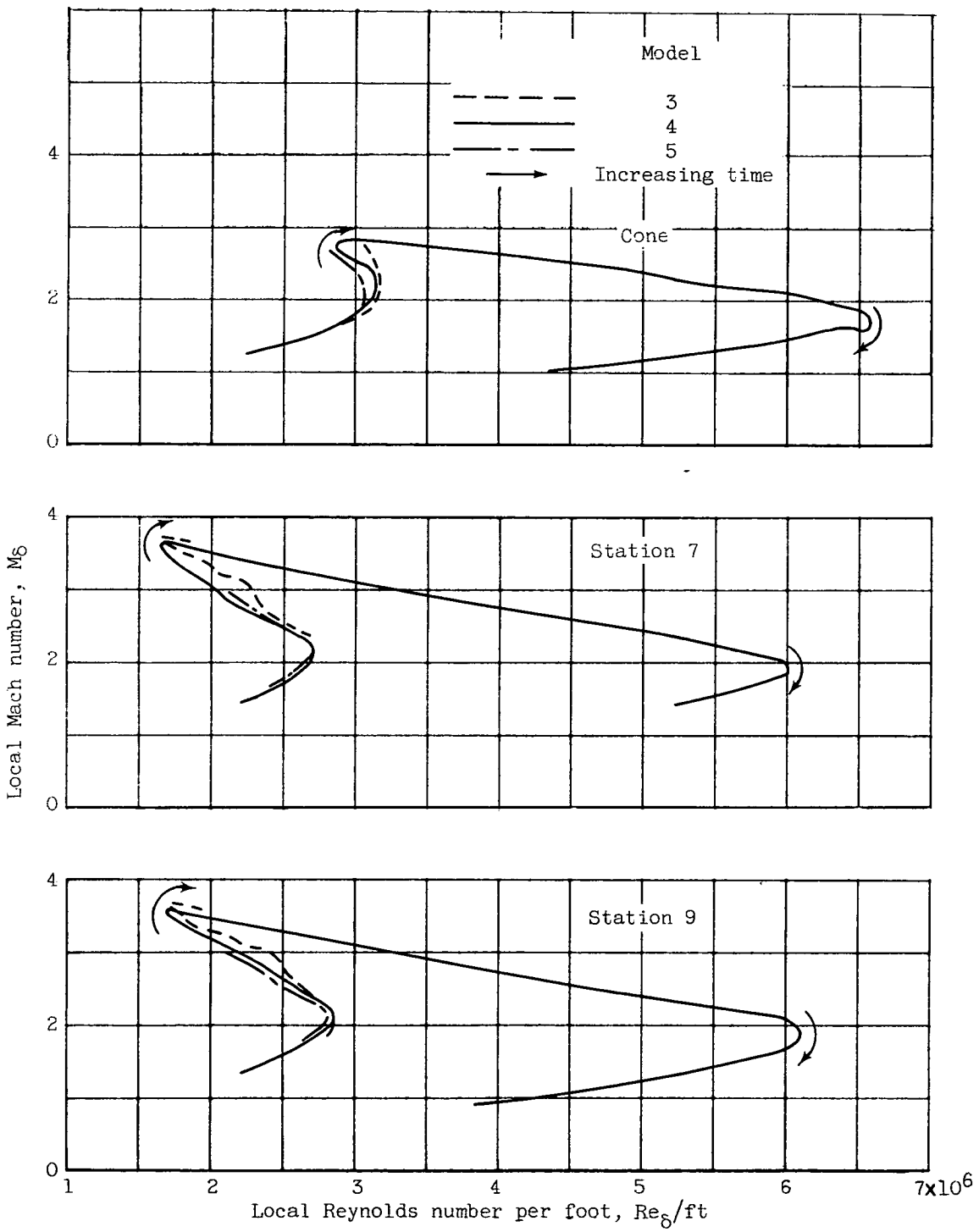

Figure 26. - Comparison of local flow conditions on the cone and at stations 7 and 9 for models 3, 4, and 5.

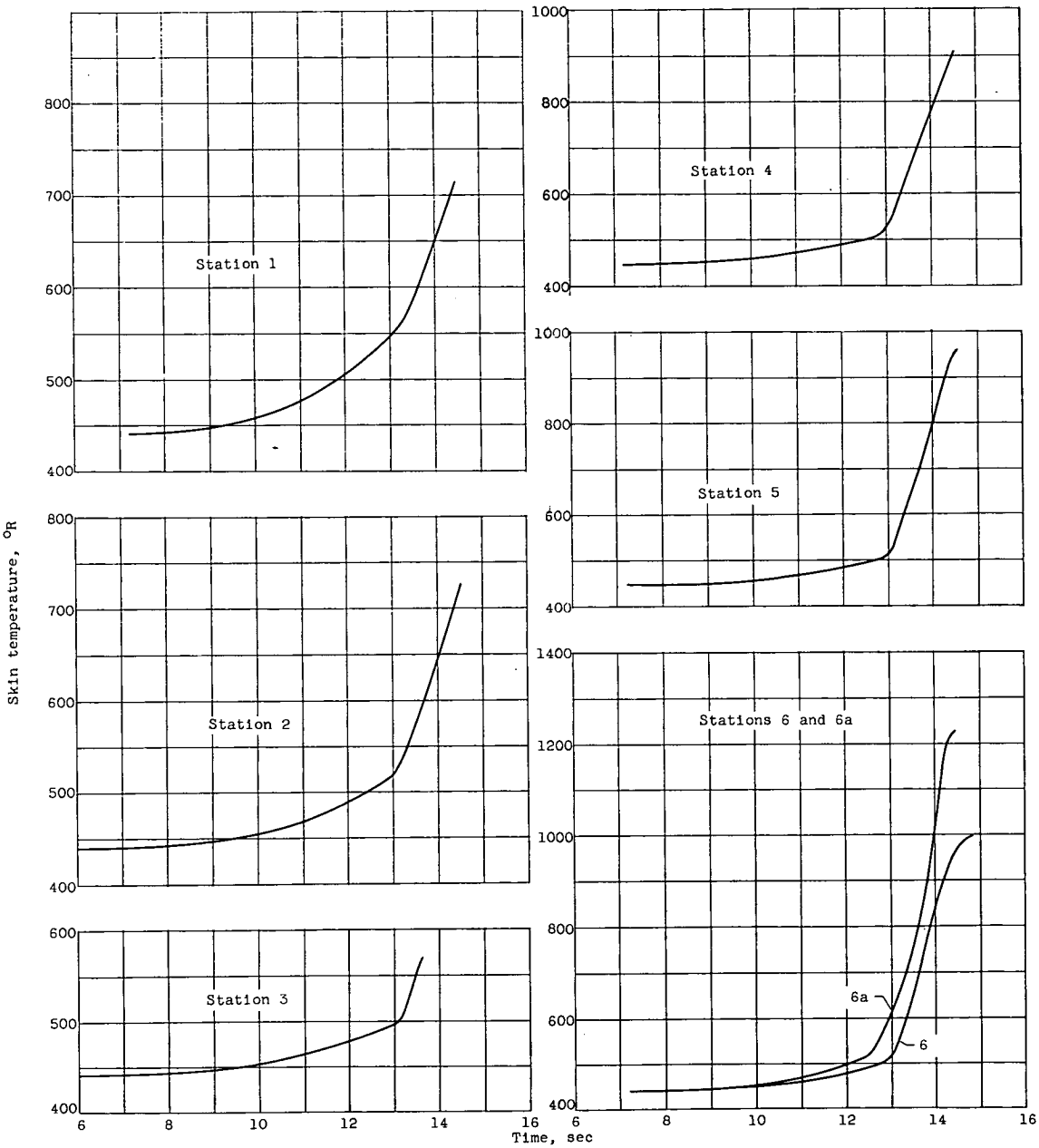

(a) Stations on cone.

Figure 27. - Time history of measured skin temperature for model 3 (50-microin. average roughness).

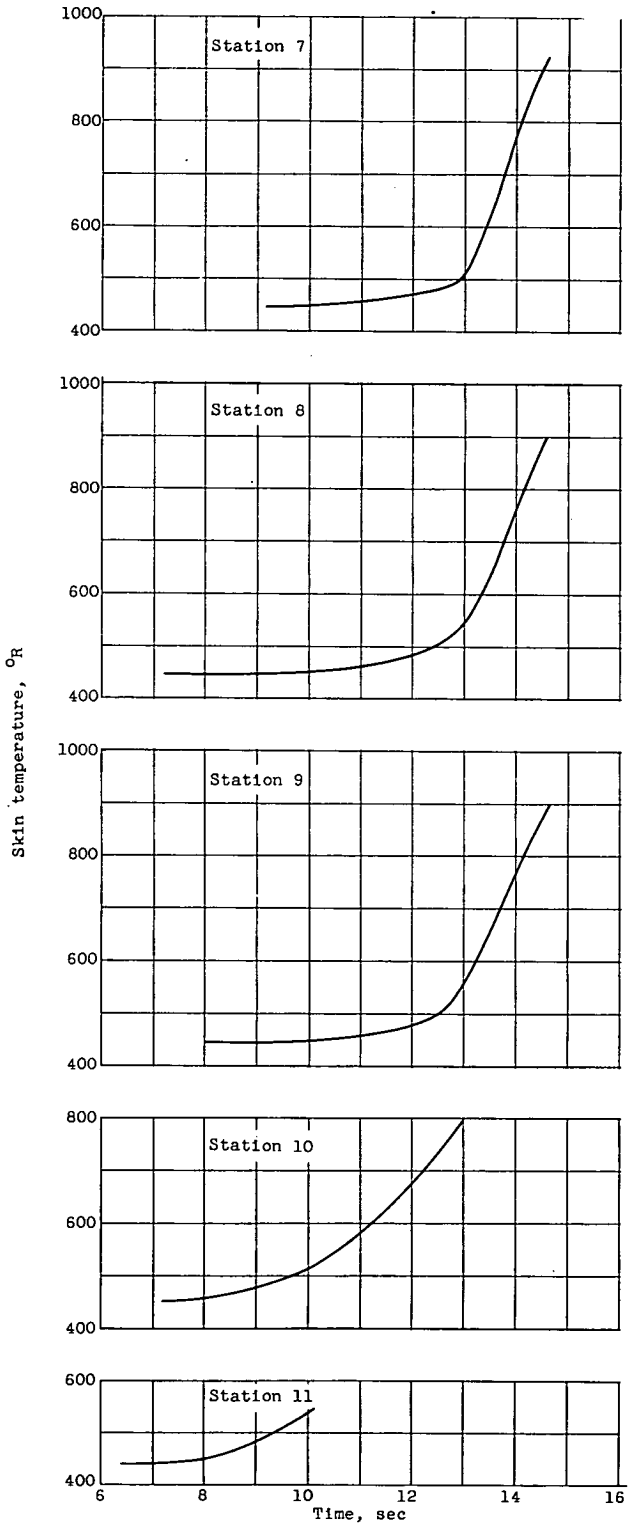

(b) Stations on cylinder and flared afterbody.

Figure 27. - Concluded. Time history of measured skin temperature for model 3 (50-microin. average roughness).

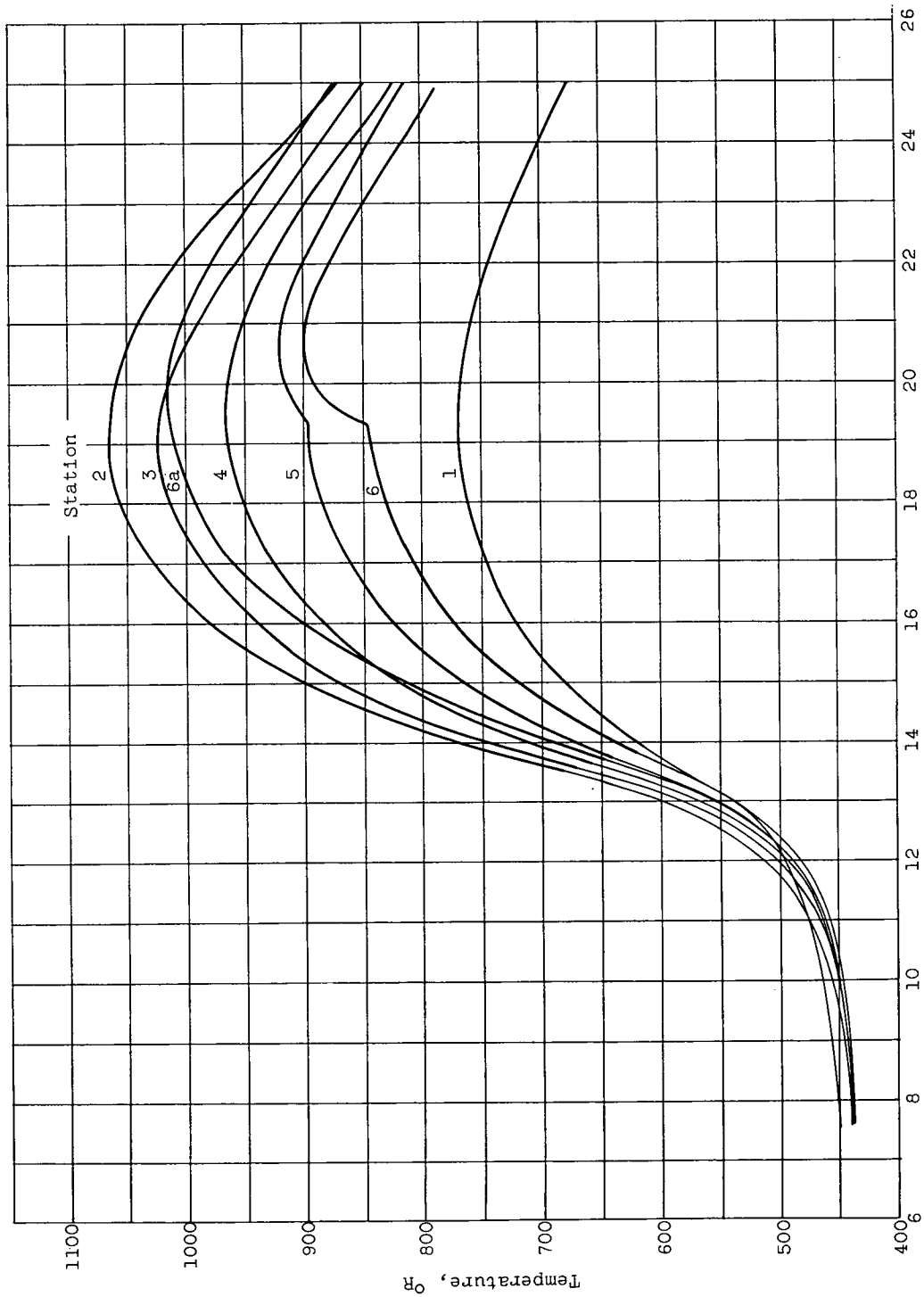

(a) Stations on cone.

Figure 28. - Time history of measured skin temperature for model 4 (2-microin. average roughness).

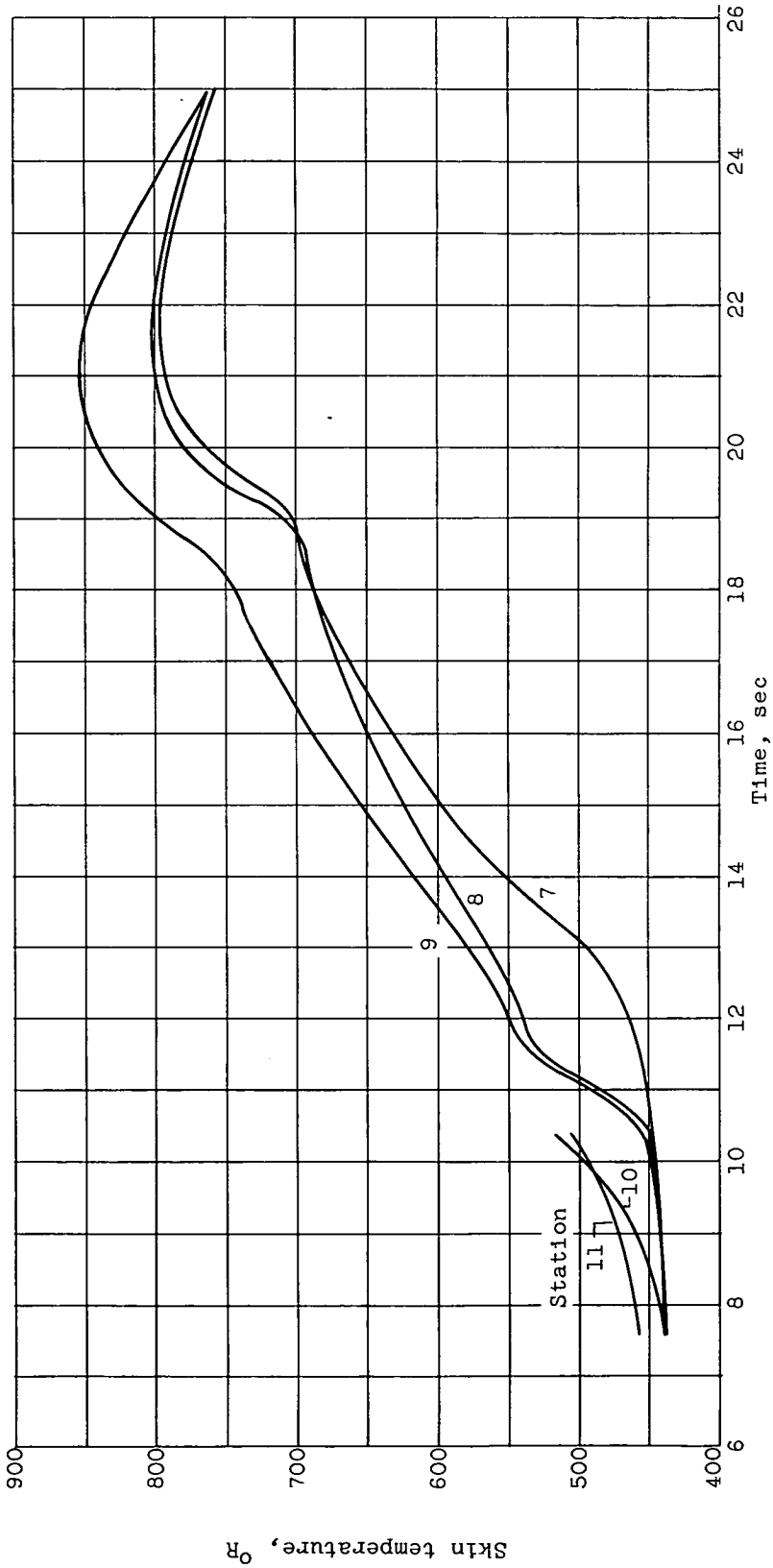

(b) Stations on cylinder and flared afterbody.

Figure 28. - Concluded. Time history of measured skin temperature for model 4 (2-microin. average roughness).

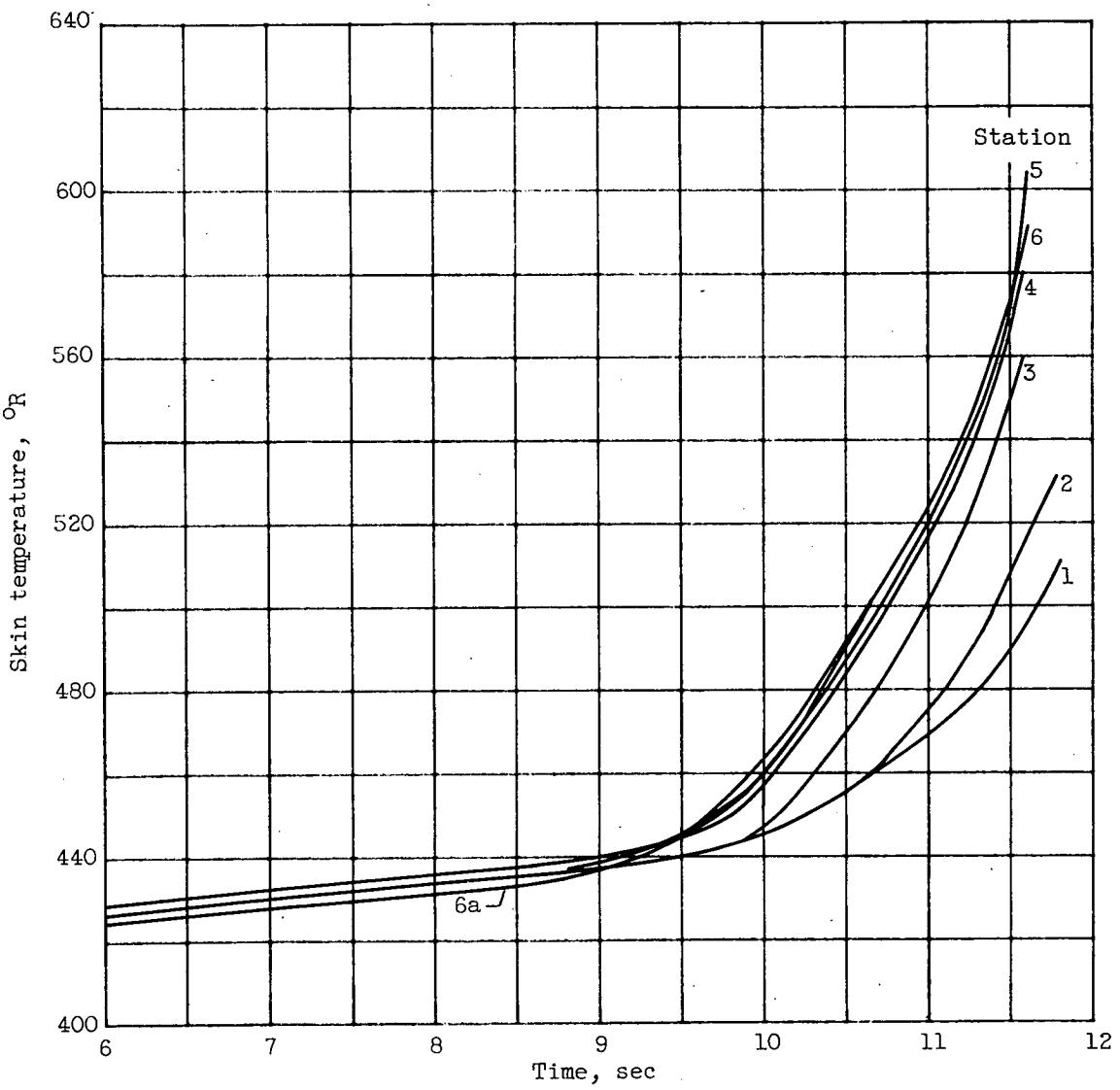

(a) Stations on cone.

Figure 29. - Time history of measured skin temperature for model 5 (20-microin. average roughness).

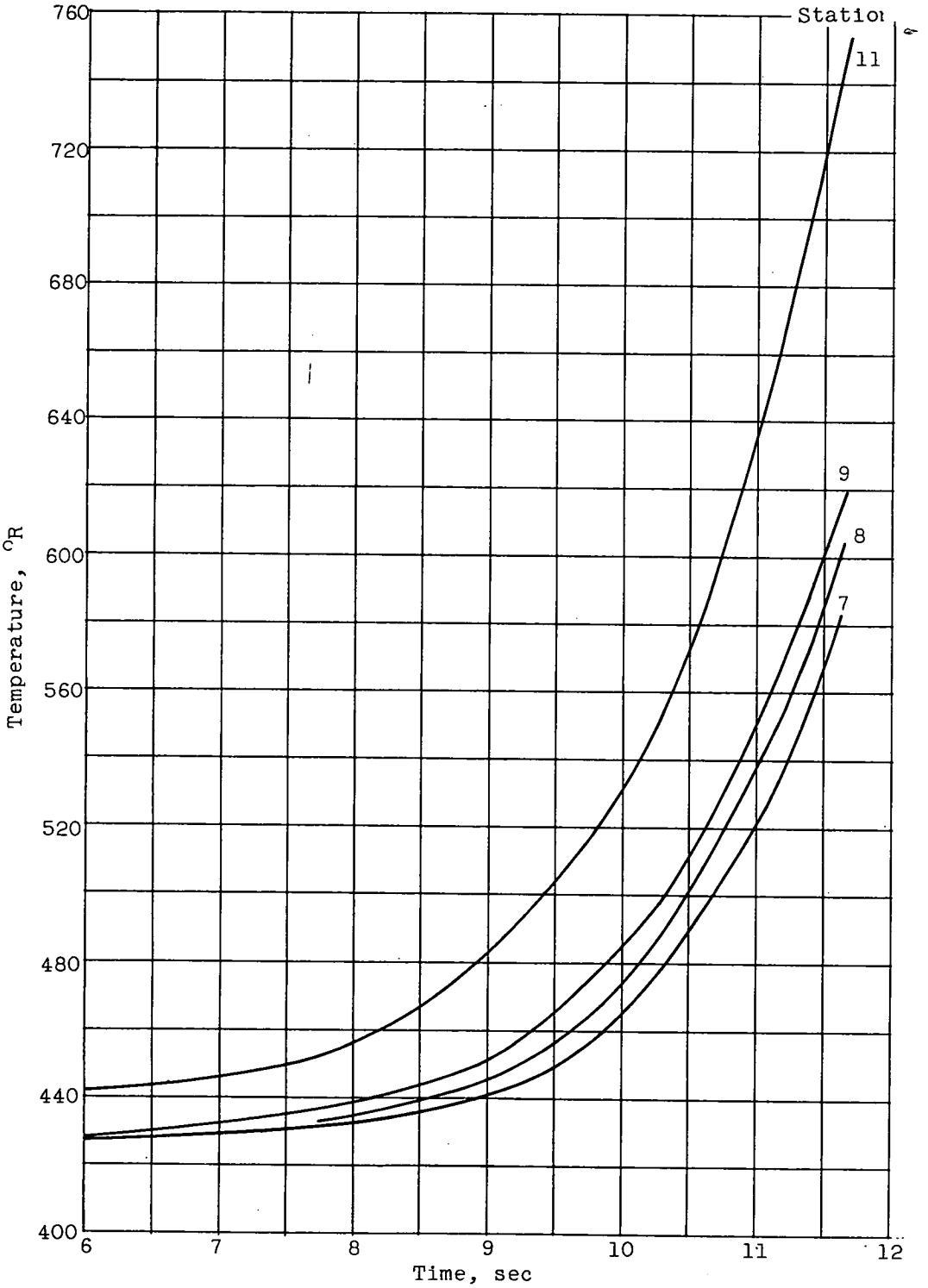

(b) Stations on cylinder and flared afterbody.

Figure 29. - Concluded. Time history of measured skin temperature for model 5 (20-microin. average roughness).

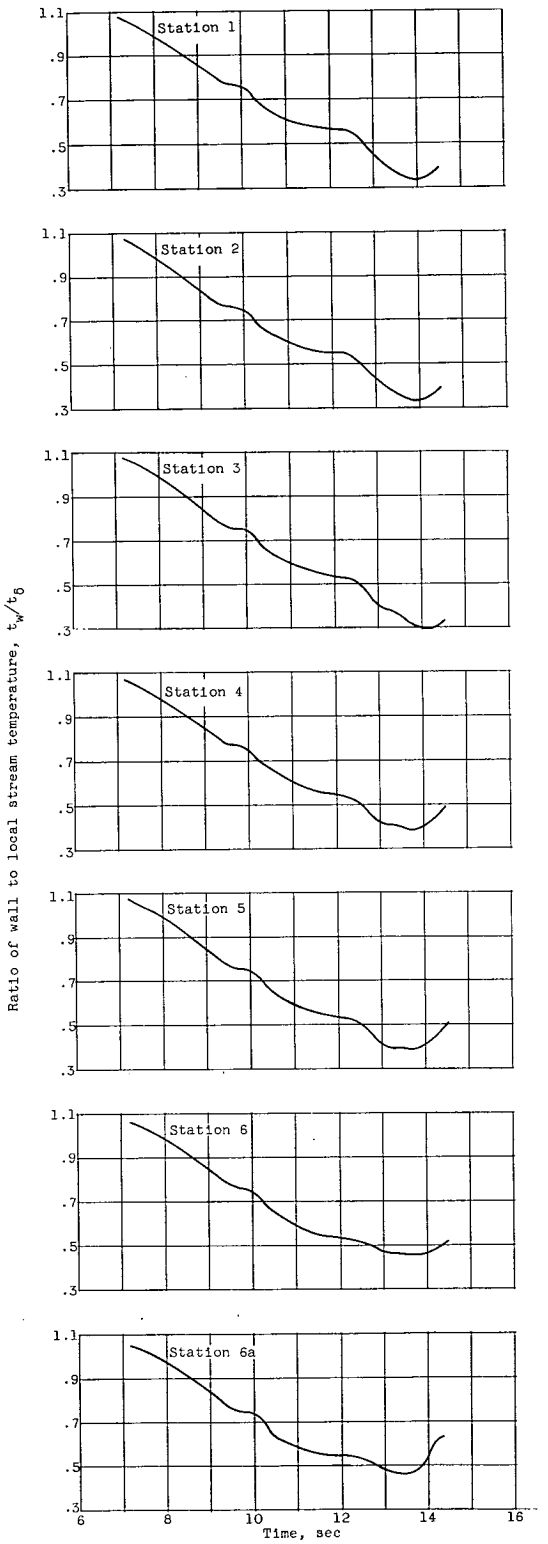

(a) Stations on cone.

Figure 30. - Time history of local temperature ratio for model 3 (50-microin. average roughness).

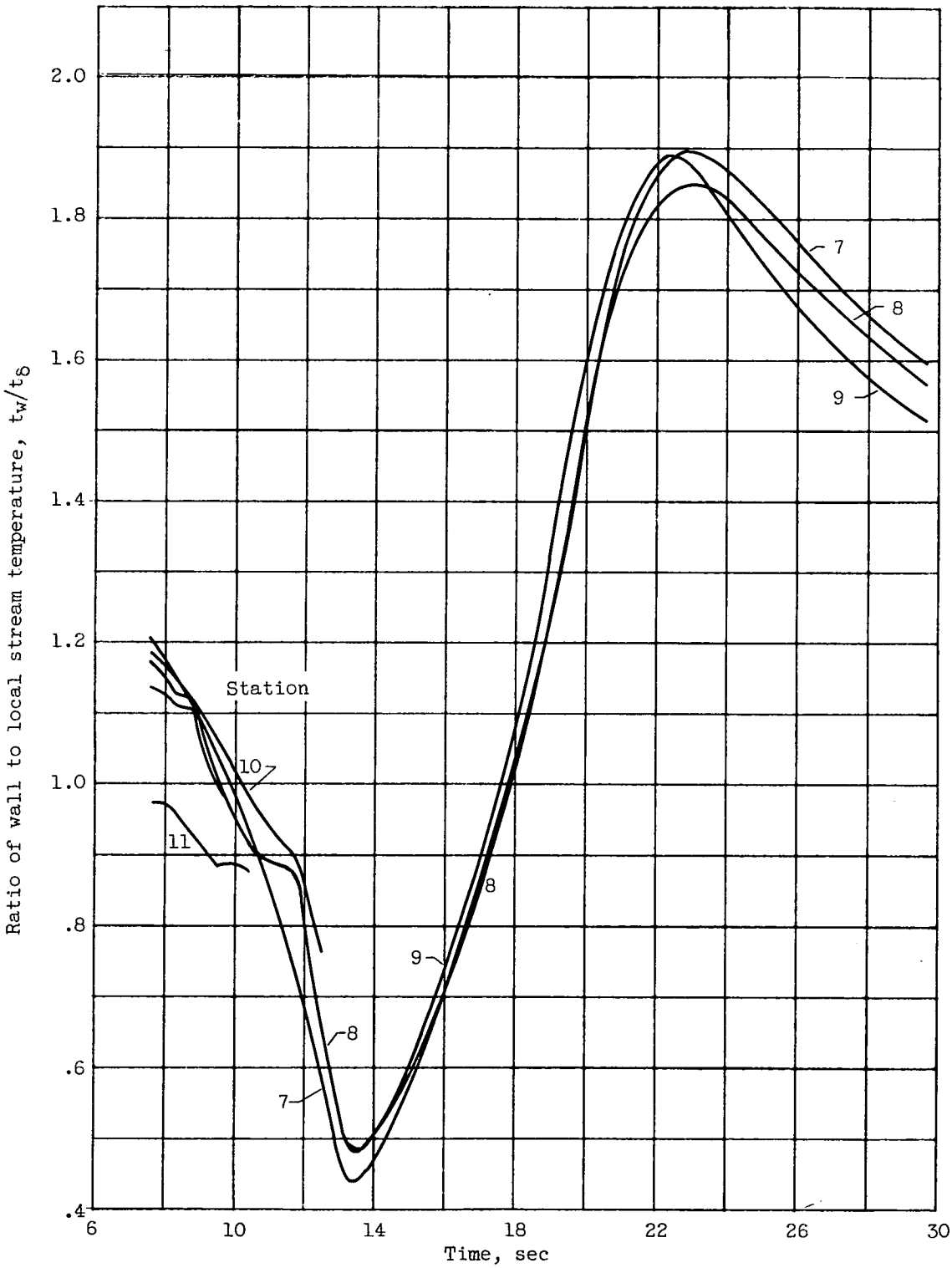

(b) Stations on cylinder and flared afterbody.

Figure 31. - Concluded. Time history of ratio of wall to local stream temperature for model 4 (2-microin. average roughness).

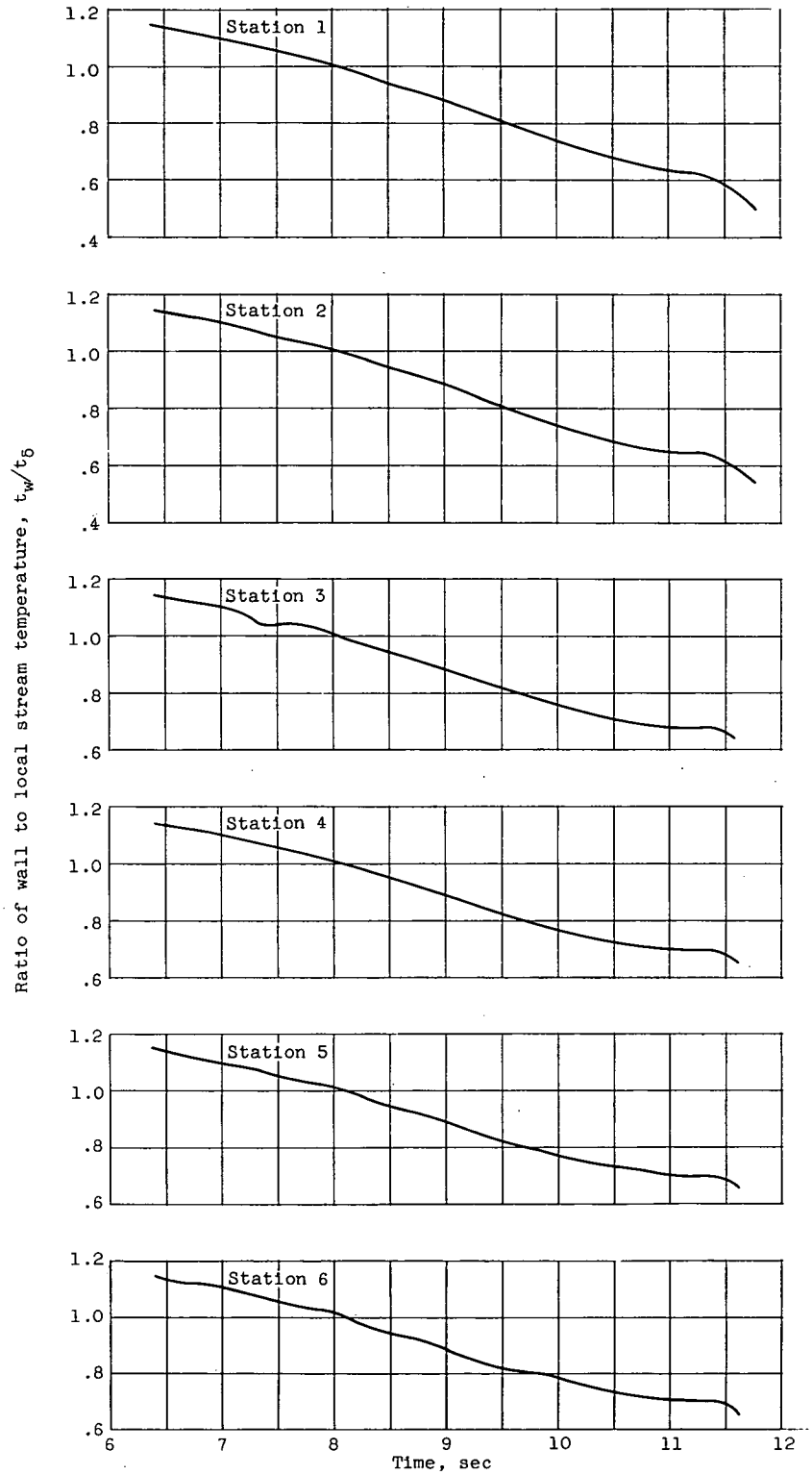

(a) Stations on cone.

Figure 32. - Time history of local temperature ratio for model 5 (20-microin. average roughness).

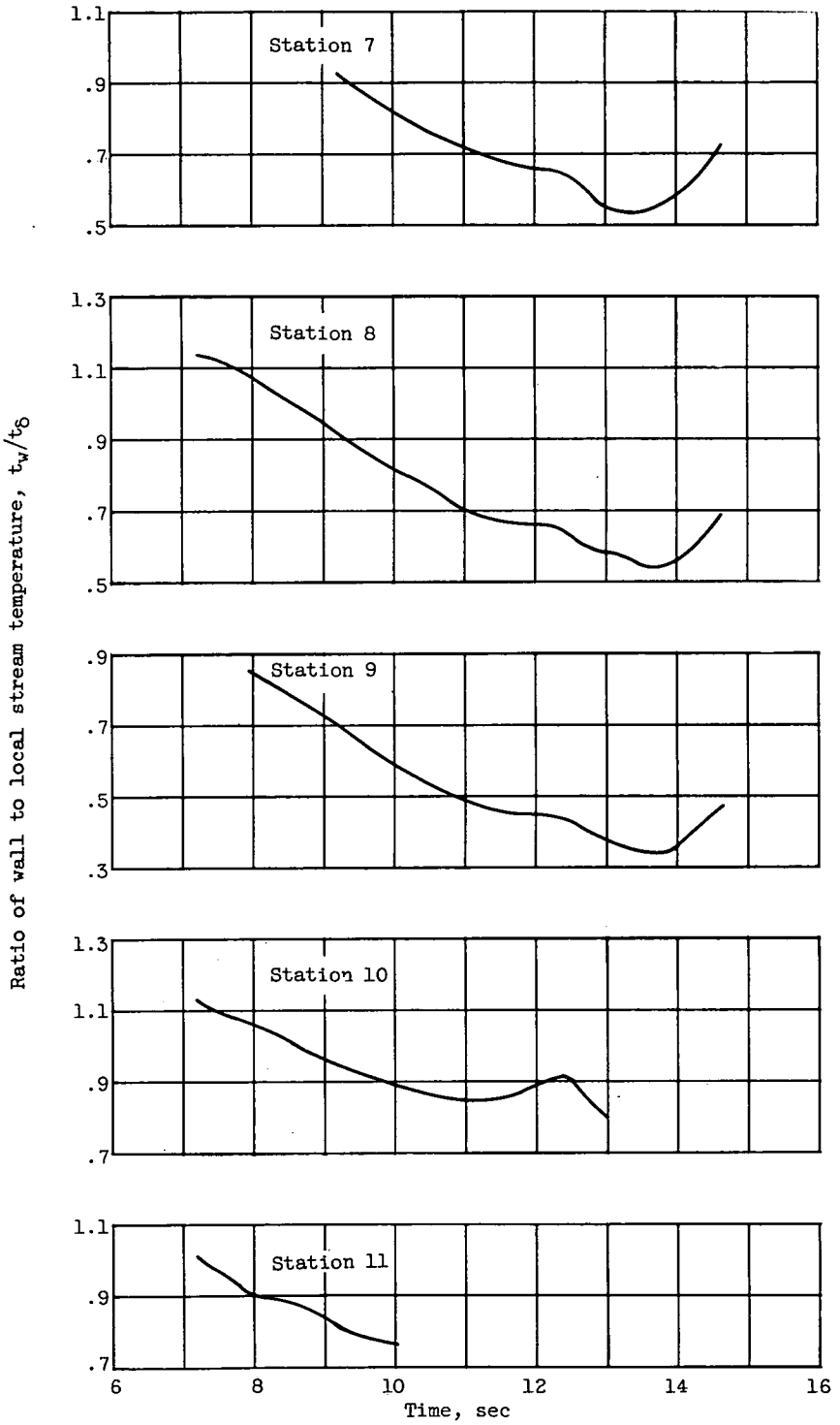

(b) Stations on cylinder and flared afterbody.

Figure 30. - Concluded. Time history of local temperature ratio for model 3 (50-microin. average roughness).

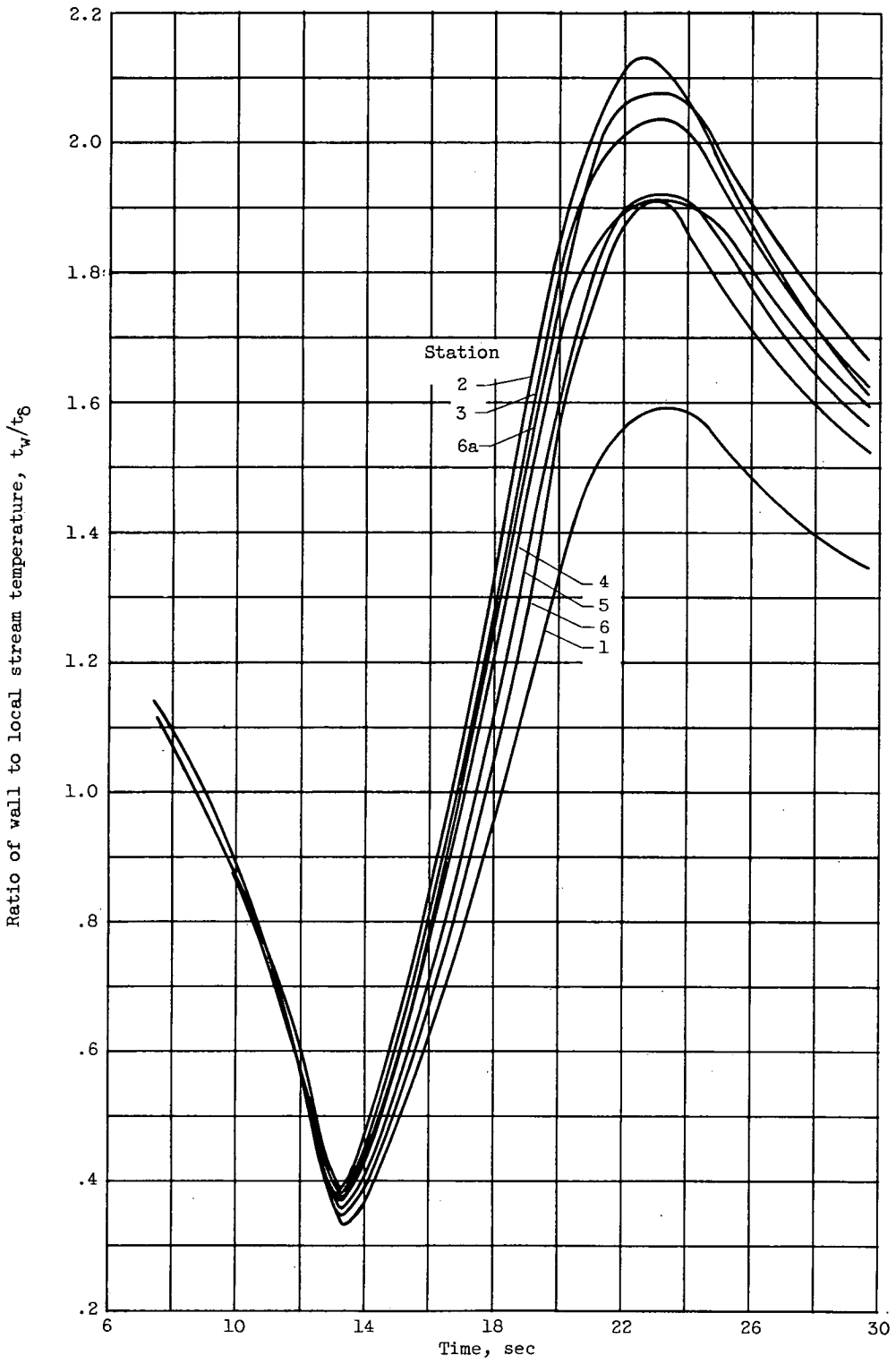

(a) Stations on cone.

Figure 31. - Time history of ratio of wall to local stream temperature for model 4 (2-microin. average roughness).

A

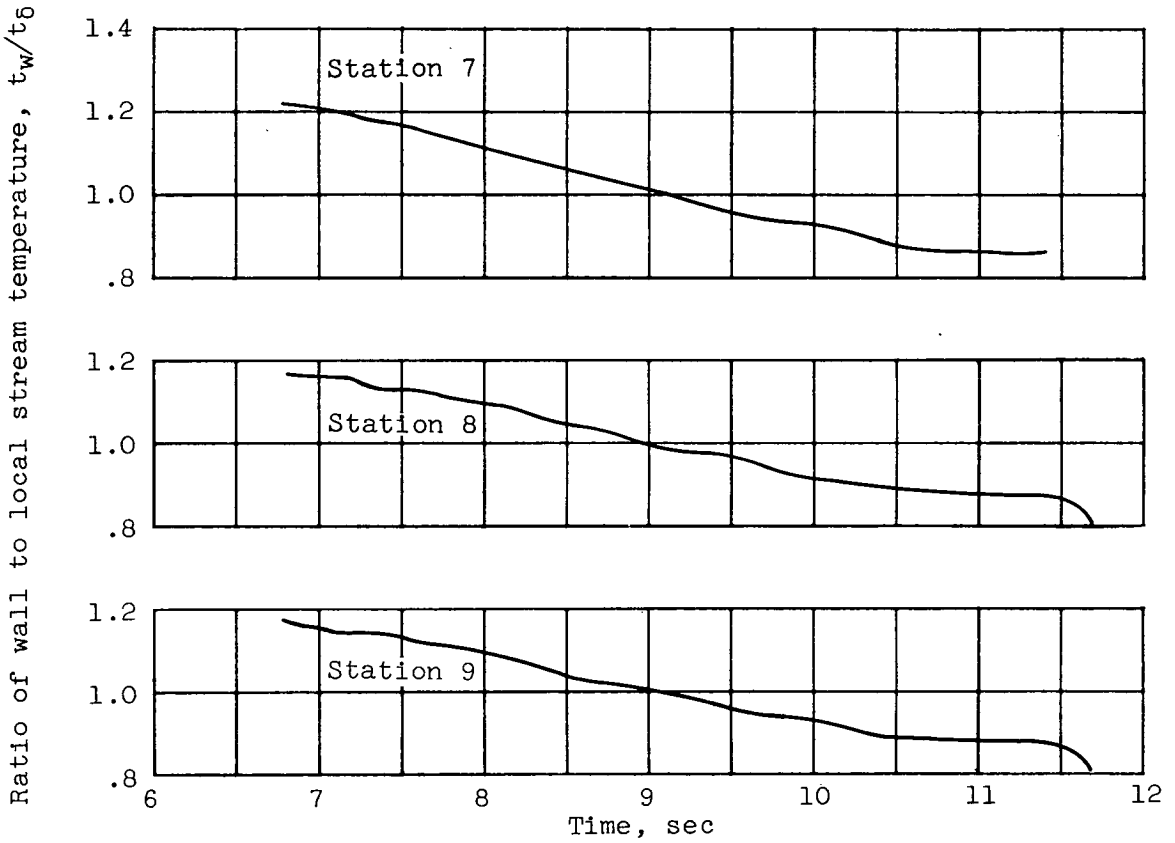

(b) Stations on cylinder.

Figure 32. - Concluded. Time history of local temperature ratio for model 5 (20-microin. average roughness).